# Crustal structure, restoration and evolution of the Greater Himalaya in Nepal–South Tibet: implications for channel flow and ductile extrusion of the middle crust

M. P. SEARLE[1], R. D. LAW[2] & M. J. JESSUP[2]

[1]*Department of Earth Sciences, Oxford University, Parks Road, Oxford, OX1 3PR, UK (e-mail: Mike.Searle@earth.ox.ac.uk)*

[2]*Department of Geosciences, Virginia Tech., Blacksburg, Virginia 24061, USA*

**Abstract:** Recent suggestions that the Greater Himalayan Sequence (GHS) represents a mid-crustal channel of low viscosity, partially molten Indian plate crust extruding southward between two major ductile shear zones, the Main Central thrust (MCT) below, and the South Tibetan detachment (STD) normal fault above, are examined, with particular reference to the Everest transect across Nepal–south Tibet. The catalyst for the early kyanite ± sillimanite metamorphism (650–680°C, 7–8 kbar, 32–30 Ma) was crustal thickening and regional Barrovian metamorphism. Later sillimanite ± cordierite metamorphism (600–680°C, 4–5 kbar, 23–17 Ma) is attributed to increased heat input and partial melting of the crust. Crustal melting occurred at relatively shallow depths (15–19 km, 4–5 kbar) in the crust. The presence of highly radiogenic Proterozoic black shales (Haimanta–Cheka Groups) at this unique stratigraphic horizon promoted melting due to the high concentration of heat-producing elements, particularly U-bearing minerals. It is suggested that crustal melting triggered channel flow and ductile extrusion of the GHS, and that when the leucogranites cooled rapidly at 17–16 Ma the flow ended, as deformation propagated southward into the Lesser Himalaya. Kinematic indicators record a dominant south-vergent simple shear component across the Greater Himalaya. An important component of pure shear is also recorded in flattening and boudinage fabrics within the STD zone, and compressed metamorphic isograds along both the STD and MCT shear zones. These kinematic factors suggest that the ductile GHS channel was subjected to subvertical thinning during southward extrusion. However, dating of the shear zones along the top and base of the channel shows that the deformation propagated outward with time over the period 20–16 Ma, expanding the extruding channel. The last brittle faulting episode occurred along the southern (structurally lower) limits of the MCT shear zone and the northern (structurally higher) limits of the STD normal fault zone. Late-stage breakback thrusting occurred along the MCT and at the back of the orogenic wedge in the Tethyan zone. Our model shows that the Himalayan–south Tibetan crust is rheologically layered, and has several major low-angle detachments that separate layers of crust and upper mantle, each deforming in different ways, at different times.

The Tibetan plateau (Fig. 1), covering an area of $>5 \times 10^6$ km, is an arid plateau with low relief and low erosion rates, and forms the largest area of high elevation (average elevation of 5023 m) and thick crust (65–80 km) on the planet (Fielding *et al.* 1994). The plateau is bordered to the south by the Himalayan range, which has a similar average elevation, but much greater topographic relief, ranging from 2000 to 8850 m, intense fluvial and glacial erosion, and high erosion rates (Duncan *et al.* 2003). The horizontal gradients in lithostatic pressure between the Tibetan plateau and the Indian shield south of the Himalaya, with its normal crustal thickness (*c.* 35–40 km) and low elevation (<1.5 km), is the driving force behind deformation involving crustal flow away from the plateau. Two major types of crustal flow have been proposed for Tibet: firstly, lower crustal flow in eastern Tibet extruding east and SE around the eastern Himalayan syntaxis; and secondly, middle crustal flow in a layer or channel extruding southward from beneath the southern part of the plateau to the Greater Himalayan range (Fig. 1).

The concept of planar channel flow (combined 'Couette flow' (simple shear) and 'Poiseuille flow' (also known as the 'pipe-flow effect') of the weak lower crust, which removes crust from beneath mountains and levels out topography, was first proposed by Bird (1991). The crustal structure of the eastern part of the Tibetan plateau has been interpreted in terms of lateral flow of a ductile layer of lower crust by several authors (Royden *et al.* 1997; Clark & Royden 2000). This appears to be supported by GPS observations that show the ground surface of north Tibet rotating around the eastern syntaxis as far as Yunnan and Burma

*From*: LAW, R. D., SEARLE, M. P. & GODIN, L. (eds) *Channel Flow, Ductile Extrusion and Exhumation in Continental Collision Zones*. Geological Society, London, Special Publications, **268**, 355–378.
0305-8719/06/$15.00 

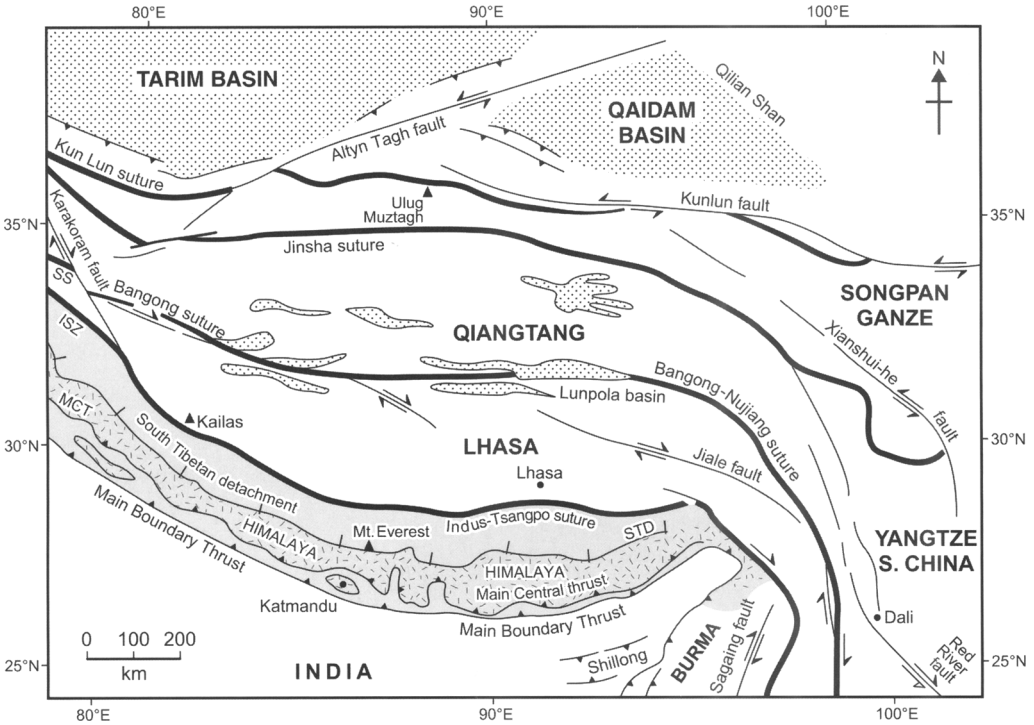


**Fig. 1.** Sketch map of the Tibetan plateau region comprising the Songpan Ganze, Qiangtang and Lhasa blocks accreted to the southern margin of Asia. Major suture zones and strike-slip faults are also shown. The Himalaya (shaded) forms the southern margin of the Tibetan plateau. The Greater Himalaya is the shaded and stippled area between the Main Central Thrust (MCT) and the South Tibetan Detachment (STD); SS, Shyok suture; ISZ, Indus-Tsangpo suture zone.

(Wang *et al.* 2001). Velocity vectors show that the south Tibetan crust and Himalaya (south of 32°N) are moving along an azimuth of 020°NNE with respect to stable Asia. North of this, the velocity vectors swing around to ENE in northern Tibet, east along the eastern margin of the plateau and continue to the south in Yunnan and northern Burma (Wang *et al.* 2001). This eastward flow of material is restricted to northern Tibet (Qiangtang and Kunlun terranes), north of the Jiale fault and south of the Kunlun fault (Fig. 1). Northern Tibet has a thin, hot lithosphere, high Poissons' ratio (ratio of latitudinal to longitudinal strain), a seismic anisotropy, possibly developed by lateral flow in the mantle, a probable granulitic lower crust and abundant Tertiary–Quaternary volcanic activity (Owens & Zandt 1997; Kosarev *et al.* 1999; Hacker *et al.* 2000). Southern Tibet has a thicker, cooler lithosphere consistent with underthrusting of crust and mantle of Indian plate affinity north as far as the latitude of the Bangong suture at *c.* 32°N (Nelson *et al.* 1996; Owens & Zandt 1997).

The lower crustal flow of the Qiangtang and Songpan Ganze terranes of northern Tibet contrasts with the channel flow model for the Greater Himalaya–south Tibet crust, in which a layer of hot, ductile deforming and partially molten middle crust was extruded south from beneath the southern part of Tibet (e.g. Grujic *et al.* 1996, 2002; Beaumont *et al.* 2001, 2004; Searle *et al.* 2003; Jamieson *et al.* 2004). Here, the mid-crustal layer of Indian plate rocks is represented by the Greater Himalayan Sequence (GHS) which is exposed in areas that form most of the highest topography, and the deepest exhumed rocks, along the Himalayan arc. The lower crust, comprising Archean Indian shield granulites, has been underthrust to the north, and is relatively rigid and melt-free. Since the crust beneath the Tibetan plateau is up to 80 km thick (*c.* 20–22 kbar pressure, assuming average crustal densities) it is possible that the lower crust has transformed into eclogite beneath the Lhasa block of southern Tibet. However, whereas granulites are dry, strong and capable of supporting thick crust like Tibet, eclogites may be hydrous, and have a density similar to, or possibly even greater than, that of the upper mantle. Ultra-high temperature and near

ultra-high pressure xenoliths in young alkali basalts in central Tibet include felsic granulites and both felsic and mafic eclogites, interpreted as tapping deep levels of the Tibetan crust (Hacker *et al.* 2000; Ducea *et al.* 2003).

This paper synthesizes data from the Everest transect, Tibet–Nepal in the context of the channel flow model. For the subsurface structure, we rely on the various seismic profiles from project INDEPTH (e.g. Nelson *et al.* 1996; Alsdorf *et al.* 1998; Hauck *et al.* 1998). For the surface geological mapping we use our data (e.g. Searle 1999*a*, *b*, 2003; Searle *et al.* 2002, 2003) as well as that of Lombardo *et al.* (1993), Carosi *et al.* (1998, 1999*a*, *b*), and for the microstructural interpretation we use the data from Law *et al.* (2004). We attempt a restoration of the entire Nepal–south Tibet GHS and use this restored section as a template to determine the protoliths of GHS rocks, the depth of melting of the Everest leucogranites, and the thrust and normal fault trajectories. Finally, we discuss the role of the South Tibetan Detachment (STD) normal faults as a passive roof fault during channel extrusion, and the role of the Main Central Thrust (MCT) in the extrusion and exhumation of the GHS.

## Greater Himalayan Sequence

The GHS, as exposed along the High Himalaya, is composed of a mid-crustal layer of high-grade metamorphic rocks and migmatites with sheets of crustal melt leucogranites prominent along the higher structural levels. The upper contact of the GHS is a low-angle normal fault system, the STD, which generally dips north (5–20°), beneath the Tibetan plateau (Burg 1983; Burg *et al.* 1984; Burchfiel *et al.* 1992; Searle *et al.* 1997). The lower boundary of the GHS is a high strain ductile shear zone, the MCT, which is coincident with a zone of inverted metamorphic isograds from kyanite grade down to biotite–chlorite grade (Hubbard 1996; Stephenson *et al.* 2000, 2001). The MCT also dips at low angles to the north and places Proterozoic and Palaeozoic rocks, metamorphosed during the Himalayan orogeny, south over Lesser Himalayan thrust sheets, which were largely unaffected by Himalayan metamorphism (Gansser 1964, 1983; Hodges 2000; Searle & Godin 2003).

The large-scale structure and pressure–temperature (P–T) constraints across the GHS have led to numerous thermal–mechanical models (e.g. Searle & Rex 1989; Hodges *et al.* 1992; Harrison *et al.* 1998; Searle *et al.* 1999*b*). Several recent papers interpreted the structural and thermal data from the GHS in terms of a channel flow model, whereby the middle crust was extruded southwards between coeval thrust- and normal-sense shear zones (Grujic *et al.* 1996, 2002; Beaumont *et al.* 2001, 2004; Searle *et al.* 2002, 2003; Searle & Szulc 2005). Although these models differ in some aspects along the strike of the mountain range, several first-order field- and laboratory-based data sets form the basis for meaningful models (see next section). Figure 2a and b show a map of the Nepal–South Tibet Himalaya, and a cross-section across the STD in the Everest region. Figure 2c is a restoration of the profile in Figure 2b using pressure-depth constraints from thermobarometry of footwall gneisses and assuming a constant dip of the STD (Searle *et al.* 2002, 2003). These authors suggested horizontal transport or flow of at least 100 km (possibly as much as 200 km) of GHS rocks along the footwall of a passive roof fault, the STD, during ductile channel flow during the Miocene.

The thermal structure of the Greater Himalaya has been interpreted with the help of petrologic and thermobarometric data. P–T profiles across the GHS generally show an inversion of temperature and pressure across the narrow MCT zone (e.g. Hubbard 1996; Searle *et al.* 1999*b*, 2003; Stephenson *et al.* 2000, 2001). Structurally above the kyanite-grade rocks, the Everest section shows a 50 km horizontal width of sillimanite-grade gneisses (Hubbard 1989, 1996; Simpson 2002; Searle *et al.* 2003). Temperatures remain high for 50 km along a north–south profile from the footwall of the STD at Rongbuk south as far as Karikhola, south of Lukla. Pressures are highest (7–8 kbar) in the south above the MCT zone and drop off to the north to 4–5 kbar (Searle *et al.* 2003, fig. 8). Pressures of Everest greenschist rocks above the Lhotse detachment are poorly constrained, but they must be relatively low (<3 kbar) because of the low metamorphic grade (upper greenschist facies). Recent discoveries of staurolite-grade schists from the south face of Lhotse (Jessup *et al.* 2004) suggest that metamorphism decreases up-structural section along the top of the GHS slab in a structural style similar to that observed in Zanskar (Searle *et al.* 1992, 1999*b*).

Several authors have suggested that metamorphic isograds were affected by crustal-scale post-peak metamorphic folding and shearing (Searle & Rex 1989; Hubbard 1996; Walker *et al.* 1999; Stephenson *et al.* 2000, 2001). At least in the NW Himalaya, it can be demonstrated that isograds were inverted by south-vergent folding and associated simple shear along the MCT zone at the base of the extruding layer. Metamorphic isograds at the top of the GHS extruding layer are right-way-up and affected by post-metamorphic normal-sense shearing and flattening (Searle & Rex 1989; Dezes *et al.* 1999; Walker *et al.* 1999;

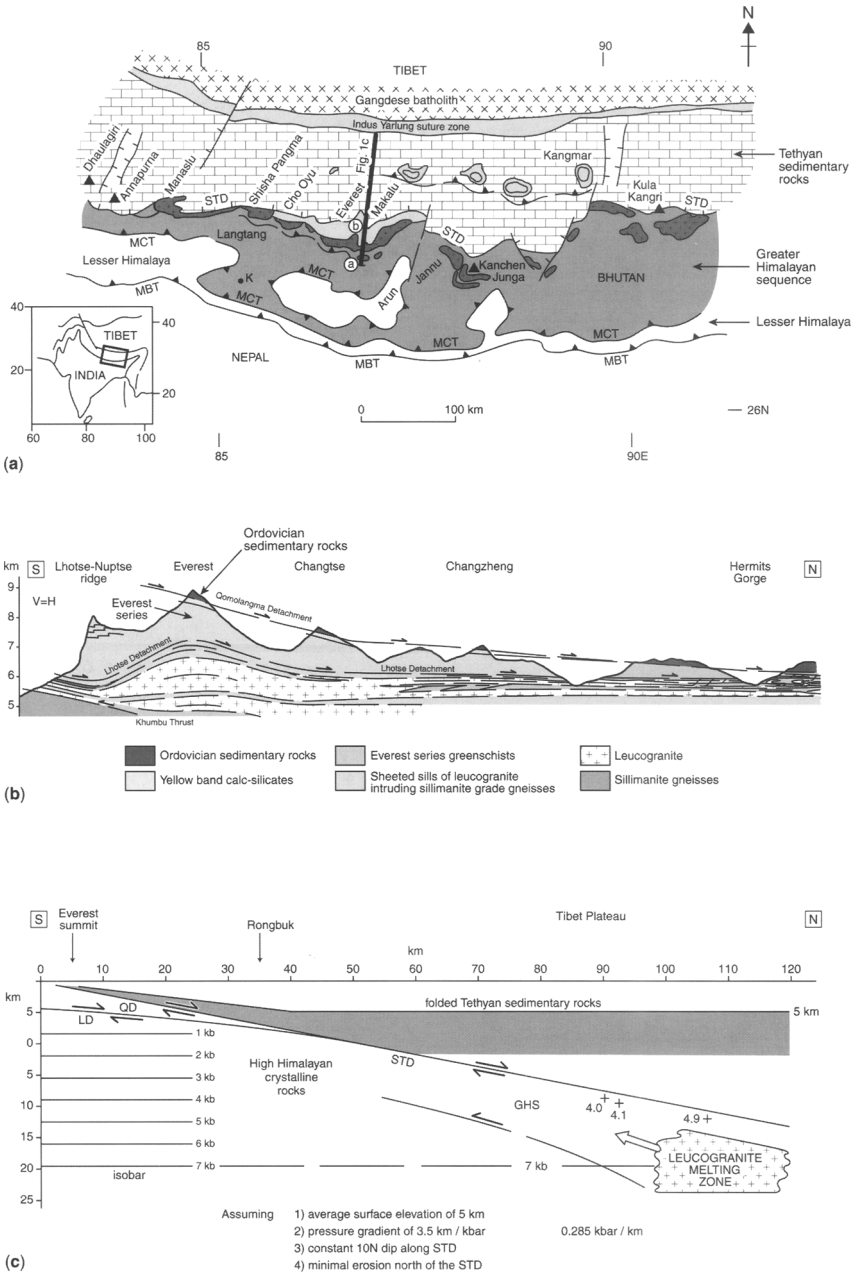


**Fig. 2.** (**a**) Geological map of the central Himalaya in Nepal, Sikkim, Bhutan and south Tibet. K, Kathmandu; MBT, Main Boundary Thrust; MCT, Main Central Thrust, (**b**) Geological section across the Everest–Rongbuk profile, marked a and b on (a) (after Searle 2003); vertical and horizontal scales are equal. (**c**) Restoration of the Everest profile along the line of section marked on (a) after Searle *et al.* (2002, 2003). The Qomolangma Detachment (QD) and Lhotse Detachment (LD) are part of the South Tibetan Detachment system of low-angle normal faults. Crosses mark the restored positions and depths of three samples from Kala Patar and Pumori, 2 km SW of Everest, which record pressures of 4.0, 4.1 and 4.9 kbar. Using a mean 10° dip of the STD passive roof fault, the relative southward displacement of footwall Greater Himalayan sequence (GHS) rocks is 90–108 km. The true dip of the STD on the north face of Everest is between 3 and 5° N; at this angle the relative displacement along the STD would be 180–216 km. The approximate depth and original position of Everest leucogranites prior to emplacement beneath the passive roof fault is also shown.

Jessup *et al.* 2004). In many parts of the Garhwal and Nepal Himalaya, late-stage brittle normal faulting has cut out the flattened and sheared right-way-up isograds at the top of the GHS layer, and the STD fault places unmetamorphosed Palaeozoic sediments directly on top of sillimanite-grade gneisses and/or leucogranites (e.g. Shisha Pangma (Searle *et al.* 1997), Garhwal (Searle *et al.* 1999*a*), Rongbuk valley (Hodges *et al.* 1998; Murphy & Harrison 1999; Searle 1999*a*; Searle *et al.* 2003) and Annapurna (Godin *et al.* 2001)).

Uniform P–T conditions of the sillimanite-grade gneisses along the Everest transect between the MCT zone at the base and the Lhotse detachment at the top, together with the lack of major structural discontinuities (except the Khumbu thrust; Searle 1999*a*, *b*) suggest that the GHS acted as a relatively homogeneous high-temperature, partially molten slab during the early Miocene. This thermal structure supports the channel flow model (Fig. 3), in which the ductile deforming channel is flowing south, bounded by major crustal-scale, low-angle ductile shear zones both below (thrust-related) and above (normal sense of shear). The timing of motion along the MCT zone along the base, and the STD zone along the top of the channel, has been extensively reviewed (Hodges *et al.* 1992; Hodges 2000; Searle *et al.* 2003; Searle & Godin 2003; Godin *et al.* 2006*a*). Both ductile shear zones were active during the early Miocene (23–15 Ma) and hornblende and mica ages are consistently older than 16–14 Ma, providing a minimum time constraint on when both shear zones were exhumed from the ductile into the brittle regime. It is possible that both shear zones are still active (e.g. Hodges *et al.* 2001). Evidence for this is the major difference in geomorphology and relief across both the bounding shear zones, evidence for young and recent motion along the lower MCT thrusts coincident with knick-points in the rivers, and the fact that the highest topography occurs largely across the GHS.

## Himalayan channel flow model

In the western Himalaya, several studies combining structural mapping with thermobarometry show that metamorphic isograds were folded after peak metamorphism, resulting in a right-way-up metamorphic sequence along the top of the GHS beneath the Zanskar shear zone (ZSZ), and an inverted metamorphic sequence along the MCT zone at the base of the slab (Searle & Rex 1989; Searle *et al.* 1992, 1999*b*; Walker *et al.* 1999; Dezes *et al.* 1999; Stephenson *et al.* 2000, 2001; Robyr *et al.* 2002; Vannay *et al.* 2004). Peak sillimanite + K-feldspar-grade metamorphism was concomitant with partial melting at *c.* 22–20 Ma (Noble & Searle 1995). The resulting 5–10 km thickness of migmatites, with abundant leucogranite sills, formed by dehydration melting of muscovite in the underlying metapelites at 4–7 kbar and 650–750°C (Searle *et al.* 1992, 2003). The right-way-up isograds along the footwall of the ZSZ were mapped, linking with the inverted isograds along the MCT hanging wall via a large-scale, SW-vergent, NW-plunging recumbent fold in western Zanskar (Searle & Rex 1989; Searle *et al.* 1992, 1999*b*; Stephenson *et al.* 2001). These data are consistent with extrusion of the GHS by channel flow and imply at least 60–100 km of motion occurring along both the bounding shear zones, the MCT and the ZSZ.

In the eastern Himalaya, a similar model was developed for the Bhutan Himalaya, where Grujic *et al.* (1996, 2002) proposed that the GHS formed the core of a low-viscosity channel extending under the Tibetan plateau. Lateral lithostatic pressure gradients produced a 'pipe-flow' effect with the highest velocities in the centre of the channel. Beaumont *et al.* (2001, 2004) presented a quantitative model in which this crustal channel was coupled to surface denudation at the High Himalayan front. In contrast, Grasemann *et al.* (1999) and Vannay & Grasemann (2001) proposed a general shear model due to the requirements of strain compatibility, whereby the centre of the channel extruded by pure shear flow, rather than the heterogeneous simple shear model invoked by Grujic *et al.* (1996).

We propose the following points as fundamental boundary conditions for the development of an orogenic channel flow model in the Himalaya (Fig. 3).

1. Channel flow is driven by the topographic and crustal thickness variation between Tibet (*c.* 5 km elevation; 70–80 km thick crust) and the Indian foreland (<1 km elevation; *c.* 35 km thick crust).
2. Presence of a mid-crustal layer, between *c.* 15 and 40 km depth, composed of ductilely deforming rocks with *in situ* partial melting (Zhao *et al.* 1993; Nelson *et al.* 1996).
3. A zone of inverted, telescoped and flattened metamorphic isograds and isotherms is present along the basal contact of the channel (Main Central Thrust zone). A ductile shear zone within kyanite-grade rocks propagates down-section to a later brittle thrust with time (Stephenson *et al.* 2000, 2001).
4. A zone of right-way-up, telescoped and flattened isograds and isotherms is present along the top of the extruding channel (STD). A ductile, normal-sense shear zone propagates upwards to a later brittle normal fault with

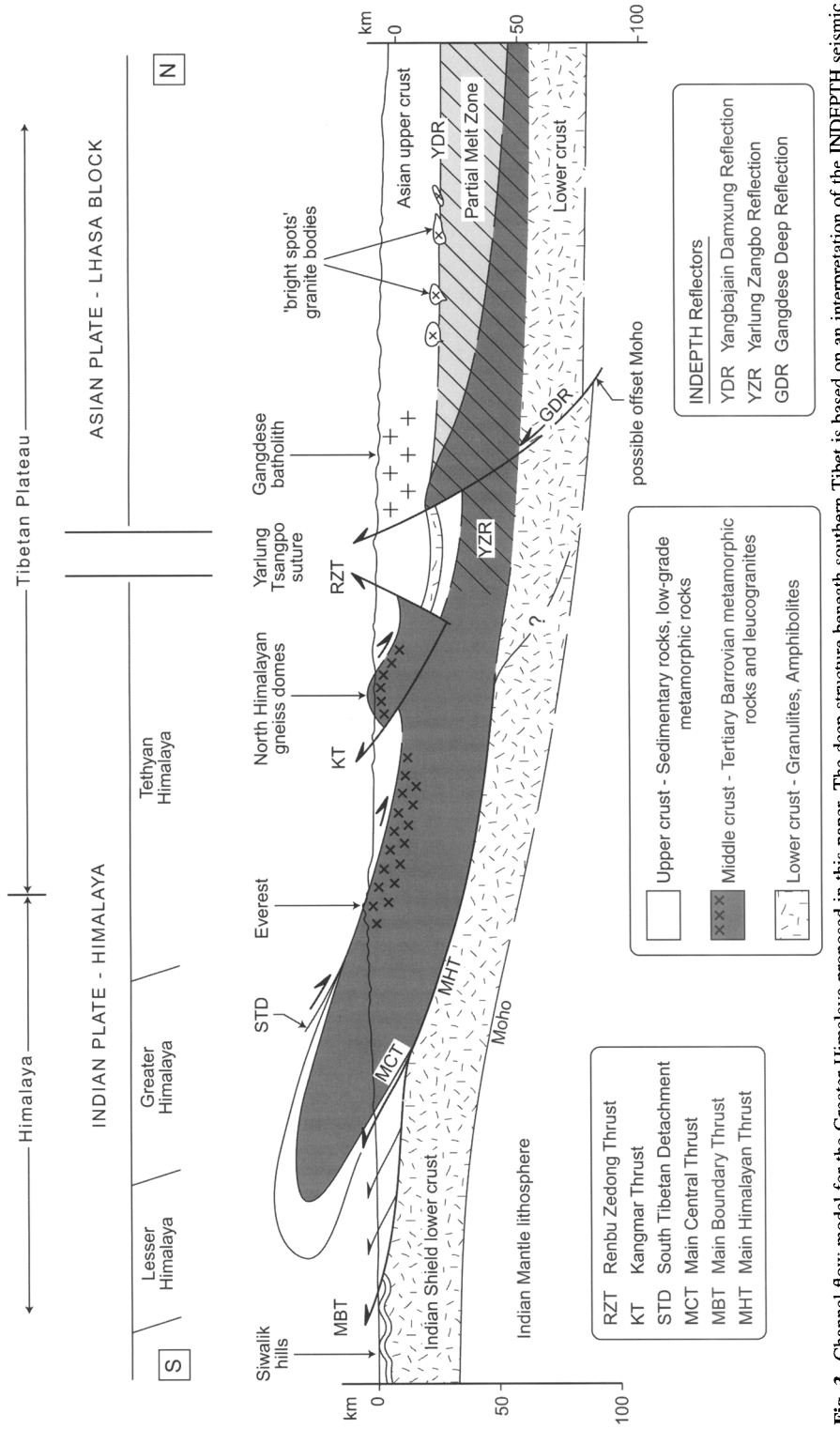


**Fig. 3.** Channel flow model for the Greater Himalaya proposed in this paper. The deep structure beneath southern Tibet is based on an interpretation of the INDEPTH seismic profile (Nelson *et al.* 1996; Hauck *et al.* 1998) and shows the reflectors bounding the partial melt layer of middle crust and the 'bright spots' interpreted here as pockets of leucogranite magma forming today. The Miocene Himalayan leucogranites are shown as small crosses along the top of the Greater Himalayan slab composed of metamorphic rocks, migmatites and *in situ* melting (shaded area). The lower crust is the relatively rigid, anhydrous granulite-facies metamorphism of the underthrust Indian shield. Also shown are the recumbent folded metamorphic isograds of the Greater Himalayan sequence (Searle & Rex 1989) linking the right-way-up metamorphism along the footwall of the STD at the top with the inverted isograds along the MCT ductile shear zone at the base of the extruding middle crust. The horizontal hatched layer in the suture zone is interpreted as a layer of ophiolitic rocks and the large crosses mark the Gangdese pre-collisional granite batholith.

time (Searle *et al.* 1992, 1997, 1999*a*, 2003; Searle & Godin 2003).

5. The two shear zones bounding the extruding channel above (STD) and below (MCT) must be structurally linked and must move synchronously (Searle & Rex 1989; Hodges *et al.* 1992, 1993, 1996).
6. Presence of partial melts (migmatites) or leucogranite magmas lubricating the flow within the extruding layer, but not cutting across the bounding brittle fault zones (Searle *et al.* 1992, 1999*a*, 2003).
7. Coupling between channel flow and surface erosion. Erosion is highest where the channel reaches the margin of the plateau in the High Himalaya (Hodges *et al.* 2001).

Figure 3 shows our interpretation of the channel flow model, based on geological (Searle 1999*a*, *b*; Searle *et al.* 2003; Law *et al.* 2004; Jessup *et al.* 2006) and geophysical (Zhao *et al.* 1993; Nelson *et al.* 1996; Hauck *et al.* 1998) data from the Nepal and south Tibet Himalaya. The shaded part of the middle crust in Figure 3 represents the channel of high-grade gneisses, migmatites and leucogranites that, during the Miocene, acted as a ductile layer sandwiched between the brittle deforming upper crust and a rigid, anhydrous, granulite-facies lower crust.

## Deep crustal structure from the INDEPTH profile

The subsurface structural interpretation beneath south Tibet is based entirely on deep seismic reflection profiling from project INDEPTH (Zhao *et al.* 1993; Nelson *et al.* 1996; Brown *et al.* 1996), combined with broadband earthquake and magnetotelluric data (Kind *et al.* 1996; Wei *et al.* 2001). The crustal structure of southern Tibet shows several reflectors, which have been successfully matched to the major faults of the Himalaya to the south, notably the STD and the Main Himalayan Thrust (MHT; Hauck *et al.* 1998; Alsdorf *et al.* 1998). The MHT is the basal detachment, which dips at about 10° north and progressively ramps up-section to the south, with both the MCT and Main Boundary Thrust (MBT) splaying off it at depth.

Magnetotelluric data (Wei *et al.* 2001) suggest that an electrically conductive layer at 15–20 km depth corresponding to zones of seismic attenuation, may reflect partial melts and/or aqueous fluids in the middle crust of southern Tibet (Nelson *et al.* 1996; Alsdorf & Nelson 1999). The 'bright spots' imaged on the INDEPTH profile beneath south Tibet have been interpreted by some as leucogranitic melts forming today, at a similar structural horizon and depth to the High Himalayan leucogranites which crystallized during the Miocene and were extruded southward to their present position along the High Himalaya (Searle *et al.* 1993, 1997, 2003; Searle 1999*a*, *b*; Gaillard *et al.* 2004). It has further been suggested that the ages of crustal melt leucogranites in the footwall of the STD decrease to the north (Wu *et al.* 1998) and that the Greater Himalayan crystalline rocks, bounded by the STD above and the MCT below, have been effectively extruded southwards from beneath the middle crust of south Tibet (Grujic *et al.* 1996, 2002; Searle 1999*a*; Searle *et al.* 2003; Searle & Szulc 2005).

Several factors such as radiogenic heating, crustal shortening and concomitant thickening could have induced the high temperatures at these mid-crustal levels beneath southern Tibet. Francheteau *et al.* (1984) measured unusually high heat flow in the lake sediments beneath Yamdrock Tso SE of Lhasa (Fig. 1), which they attributed to the presence of a magma body at 10–20 km depth. Satellite data reveal a magnetic low over Tibet indicating hot crust, and the deeper levels of the high-conductivity zone have been interpreted as a zone of *in situ* partial melting (Alsdorf & Nelson 1999). Seismological data show that relatively fast (cool) upper mantle extends from the Himalaya northwards to roughly the centre of the Tibetan plateau around the latitude of the Bangong suture (Jin *et al.* 1994; Owens & Zandt 1997; Kosarev *et al.* 1999). This has been interpreted as the northern limits of cold Indian lithosphere underthrust beneath the plateau.

## Crustal structure of the Everest transect

The surface structure of the GHS in the Everest transect is shown in Figure 4, together with U–Pb ages of metamorphic rocks and leucogranites (Simpson *et al.* 2000; Viskupic & Hodges 2001; Searle *et al.* 2003) and Th–Pb ages of Murphy & Harrison (1999) from Rongbuk, and Catlos *et al.* (2002) from the MCT zone. The structure of the profile has been presented previously (Searle 1999*a*, *b*, 2003; Searle *et al.* 2003; Law *et al.* 2004; see also Jessup *et al.* 2006, fig. 3) and only the main points pertinent to the discussion on channel flow need be repeated here. The upper part of the GHS slab in the Everest region is marked by two low-angle normal faults, which merge towards the north along the Rongbuk and Kharta valleys into one major shear zone (Searle *et al.* 2002, 2003). The structurally lower Lhotse detachment is a ductile shear zone that separates sillimanite-grade gneisses with abundant leucogranite sills beneath from lower amphibolite

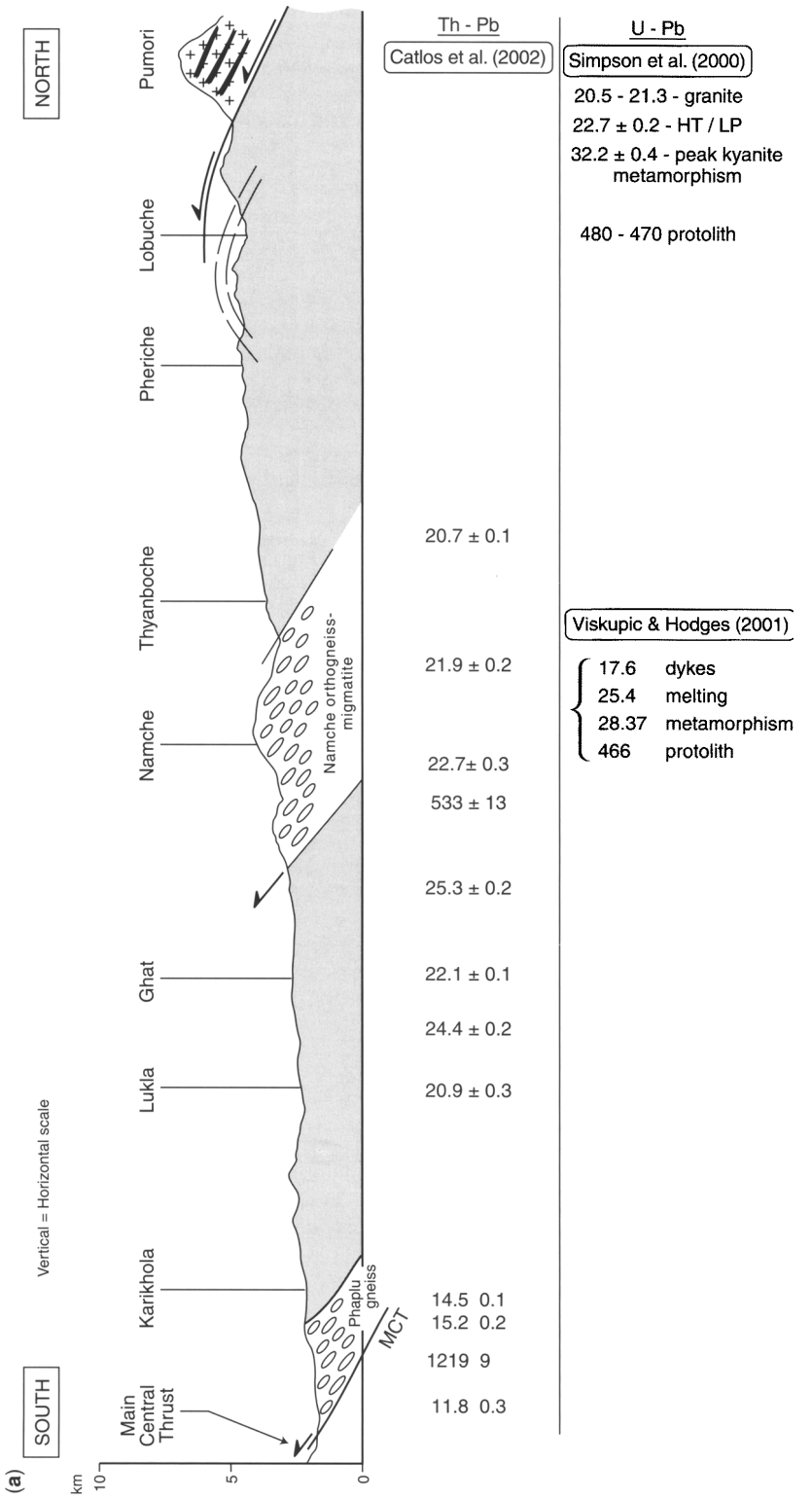


**Fig. 4.** (**a**, **b**) Cross-section through the Greater Himalayan sequence along the Everest transect from the South Tibetan detachment along the Rongbuk valley in Tibet to the Main Central Thrust zone in Nepal showing all U–Th–Pb age data from this profile. MCT, Main Central Thrust; LD, Lhotse detachment; QD, Qomolangma detachment.

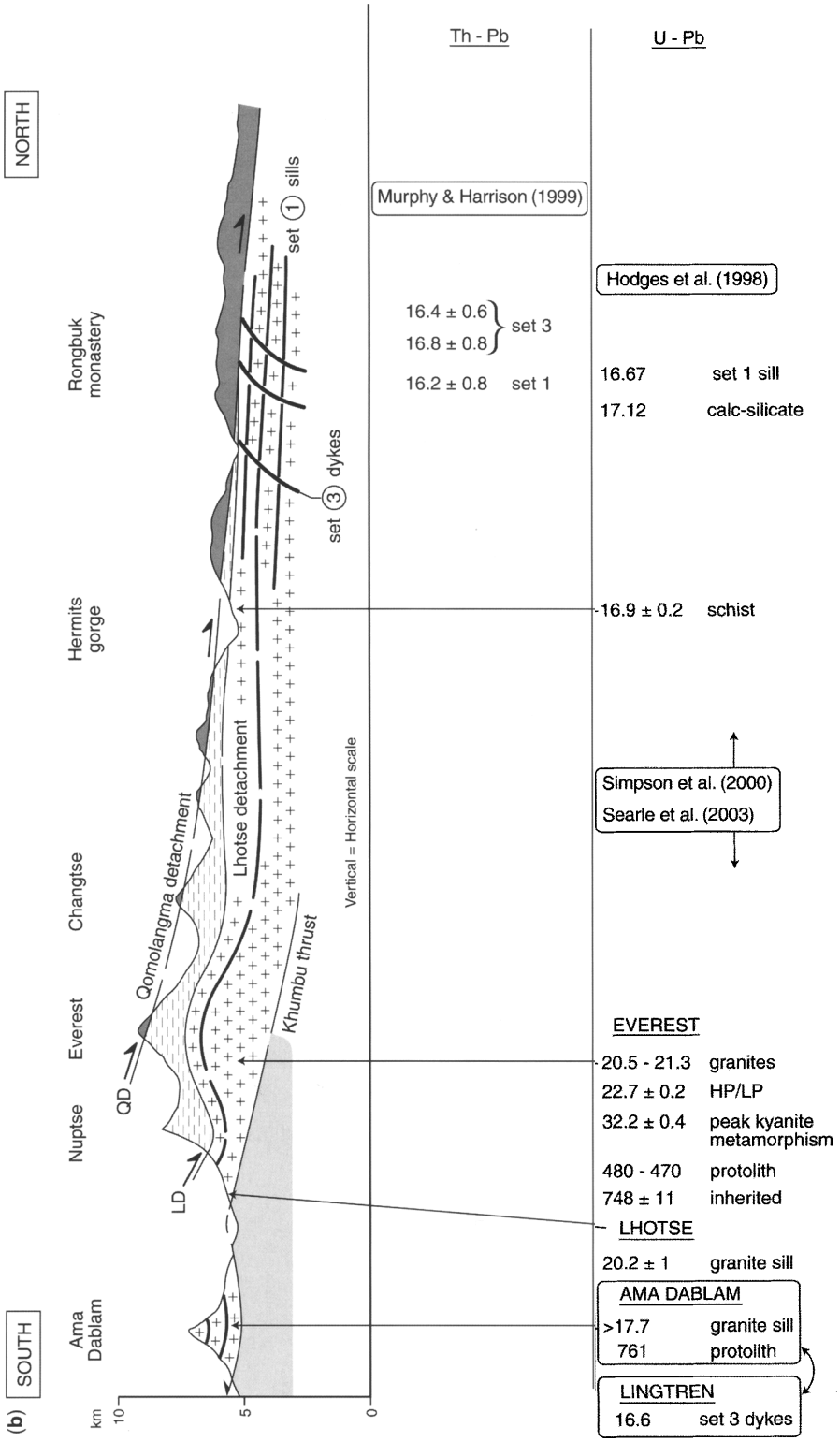


**Fig. 4.** *(Continued)*

(Jessup *et al.* 2004)–greenschist-facies pelitic and calcareous rocks (Everest series) with few, if any, leucogranites above. The structurally higher normal fault, the Qomolangma detachment, separates Everest Series metapelites beneath from unmetamorphosed Ordovician sedimentary rocks above. Beneath the Lhotse detachment a coherent leucogranite sill, up to 3.5 km thick, composed of tourmaline + biotite + muscovite ± garnet leucogranite, extends at least from the Makalu massif westwards to Cho Oyu across the lower edifice of Mount Everest and the Nuptse–Lhotse massif (Searle 1999*a*, *b*, 2003). Numerous leucogranite sills extend from the Everest massif north for at least 57 km along the Kharta and Rongbuk valleys as parallel sheets within the gneisses. Early leucogranite sills are parallel to the ductile fabrics within the gneisses, whilst a few later dykes cross-cut the fabric, but are themselves truncated by the brittle Qomolangma detachment above (Murphy & Harrison 1999; Searle *et al.* 2002, 2003).

Most of the high peaks in the Khumbu Himalaya (including the base of Cho Oyu, Gyachung Kang, Nuptse, Everest, and most of the peaks Chomolonzo, Makalu, Baruntse, Ama Dablam, Kangteiga, Tramserku) are composed of flat-lying leucogranite sills within the high-grade sillimanite gneisses (Searle, 1999*a*, *b*; Weinberg & Searle 1999; Visona & Lombardo 2002). Some sills are very narrow (<1 m), whilst others reach 1–2 km in thickness. A few interconnecting dykes link the foliation-parallel sills, but the rarity of discordant dykes implies that magma transport was dominantly along the foliation planes. In the Everest–Lhotse–Nuptse massif, the leucogranites lie above the north-dipping Khumbu Thrust (Searle 1999*a*, *b*), well exposed along the south face of Nuptse and Lhotse, which has transported these rocks south over sillimanite gneisses that contain very few leucogranites.

Along the Everest–Lukla transect in Nepal, sillimanite remains the stable aluminium silicate over the 45 km horizontal width (and >15–20 km structural depth) of the GHS, indicating that the extruding slab of middle crust had a high-temperature core during the early Miocene. Although pelites are dominant throughout this section, there are numerous horizons of calc-silicates and K-feldspar augen gneisses throughout the whole sequence down as far as the MCT zone. We apply the original definition of the MCT, and map it as the main zone of high strain separating rocks metamorphosed during the Tertiary above (Phaplu augen gneiss and structurally higher gneisses), from underlying rocks largely unmetamorphosed during the Himalayan orogeny (Lesser Himalaya). This corresponds to the lower MCT-1 position of Arita (1983) and not to the structurally higher 'MCT' (north of Karikhola, south of Lukla; Catlos *et al.* 2002). Thus, rocks previously described as 'upper Lesser Himalayan crystallines' (e.g. Catlos *et al.* 2002; Vannay *et al.* 2004) at kyanite or sillimanite grade that have P–T conditions similar to rocks higher up the section throughout the GHS slab, are here considered part of the GHS, above the MCT. The entire base of the GHS is a large-scale shear zone, corresponding to the zone of inverted metamorphic isograds, but the precise distribution of strain has yet to be determined by a detailed kinematic investigation.

## Restoration of the Everest Himalaya

Figure 5 is a schematic restoration of the Everest transect through the GHS, showing the trajectories of a number of the major faults. The restoration shows the position of the two major low-angle normal faults that cut through Everest itself: the upper Qomolangma detachment which flattens out along the top of the Ordovician 'Yellow Band'; and the lower Lhotse detachment, which bounds most of the large leucogranite sills (Searle 1999*a*, *b*; Searle *et al.* 2003). The Everest granites must have been sourced within the Proterozoic black shales that formed the protolith of the sillimanite gneisses comprising Unit 1 in the GHS, also called the Barun gneiss (Pognante & Benna 1993; Lombardo *et al.* 1993). We discard the previous 'stratigraphic' nomenclature of the GHS (e.g. Le Fort 1981; Colchen *et al.* 1986) because we believe that it oversimplifies the complex metamorphic lithologies and structure of the GHS (Searle & Godin 2003). For example, there are numerous horizons of augen gneiss (previously called Formation III) throughout the GHS from the base of the slab (Ulleri and Phaplu augen gneisses) up to the highest levels beneath the leucogranites (e.g. Pumori augen gneiss; Searle 2003). Likewise, calc-silicate bands (previously Formation II) and less common amphibolites are present at several levels throughout the GHS sequence.

The Namche K-feldspar orthogneisses, together with similar orthogneisses higher up the slab near Pumori, were intruded into the sillimanite gneisses and the metamorphosed Cambrian–Ordovician limestones–calc-silicates. The orthogneisses contain biotite, sillimanite, cordierite, quartz, plagioclase and K-feldspar. Monazite–xenotime thermochronology suggests that the original protolith crystallized at, or before, 466 Ma; metamorphism began at, or before, 28.37 Ma, and anatectic melting occurred at 25.4–24.75 Ma (Viskupic & Hodges 2001). The Namche orthogneisses are therefore interpreted as part of the suite of late Cambrian–Ordovician granitoids that intruded the Indian plate (Miller *et al.* 2001),

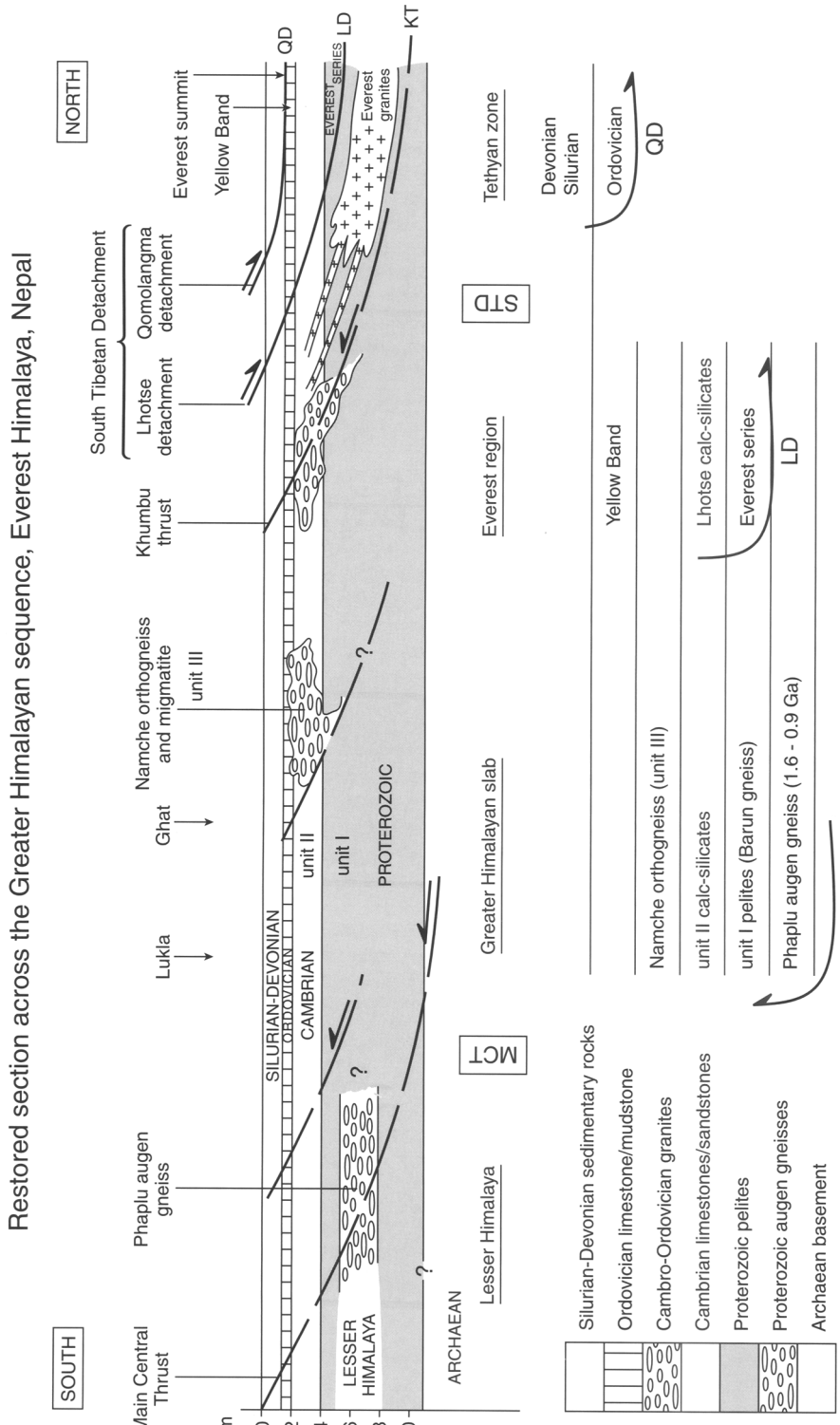


**Fig. 5.** Schematic restored section across the Greater Himalayan sequence (GHS) in the Everest Himalaya. Shaded area represents the protolith rocks of GHS mid-crustal channel. Unit I is dominantly pelitic and interpreted as metamorphosed Proterozoic shales. Minor layers of calc-silicate and amphibolite occur throughout this unit. Unit II is dominantly calc-silicate and marble, interpreted as metamorphosed Cambro-Ordovician carbonates. K-feldspar orthogneiss includes Proterozoic augen gneisses (Phaplu gneiss) and metamorphosed Cambro-Ordovician gneisses (Namche gneisses). The protolith source of the Everest leucogranites is interpreted as the Proterozoic black shale sequence beneath the Lhotse Detachment (LD) and above the Khumbu thrust (KT; Searle 1999*a*, *b*). The Qomolangma Detachment (QD) places unmetamorphosed Ordovician–Silurian sedimentary rocks on top of Ordovician greenschist-facies marbles (Yellow Band) and Everest Series pelites. The QD and LD merge to the north, off this section.

and have subsequently been metamorphosed during the Oligocene Himalayan event, resulting eventually in Miocene partial melting.

Farther south within the GHS, another prominent level of K-feldspar augen gneisses crops out near the village of Phaplu (Fig. 4). These gneisses contain K-feldspar, quartz, plagioclase, biotite and hornblende, with a metamorphic assemblage including muscovite, biotite, garnet and sillimanite. A Th–Pb monazite age of 1219 ± 9 Ma is interpreted as the age of the protolith (Catlos *et al.* 2002), significantly older than the protolith ages of K-feldspar augen gneisses higher in the section. Restoration of the section strongly suggests that the protolith of the sillimanite-grade metapelites lying structurally above the Phaplu augen gneiss was the Proterozoic Haimanta Group shales and greywackes (Fig. 5).

A final requirement from the restored section through the GHS is that the footwall and hanging wall rocks across the MCT must match up. The GHS has a sedimentary provenance, dominantly of late Proterozoic age, based on detrital zircon ages of 0.8–1.0 Ga, whereas Lesser Himalayan zircons have older 1.87–2.60 Ga ages (Parrish & Hodges 1996). However, there is no evidence of a Palaeozoic suture and no evidence of any pre-Himalayan displacement on the MCT as required by the model of DeCelles *et al.* (2000). The MCT is a thrust fault, which, upon restoration, must match footwall–hanging wall cut-off points. The difference in Nd isotope characteristics can be explained by the stratigraphic level of protolith rocks either side of the MCT seen on the restoration. The Greater Himalayan rocks above the MCT have $\varepsilon_{Nd}$ values of −16 and are clearly Proterozoic shales, not basement rocks, whereas the Lesser Himalayan rocks beneath the MCT have an average $\varepsilon_{Nd}$ value of −21.5, derived from Indian basement (Robinson *et al.* 2003). There is, however, no need to invoke a separate terrane for the GHS as in the Robinson *et al.* (2003) model; it is merely a higher stratigraphic level exposed in the restored GHS than the more southerly Lesser Himalaya.

## STD as a passive roof fault to the extruding channel

The upper boundary of the GHS channel is marked by the low-angle normal faults of the South Tibetan Detachment (STD). This detachment is an orogen-scale fault present along 2000 km of the High Himalaya from the Zanskar region of NW India to Arunachal Pradesh in the east. It places the unmetamorphosed or anchizone sedimentary rocks of the Tethyan zone above the high-grade metamorphic rocks, migmatites and leucogranites of the Greater Himalayan Series. The STD zone includes a structurally lower ductile shear zone, the Lhotse detachment, and a higher-level brittle fault, the Qomolangma detachment. In the Everest transect massive leucogranite sills occur below the structurally lower Lhotse detachment (Searle 1999*a*, *b*, 2003). The two shear zones merge towards the north to form one very large high-strain zone with leucogranite sills and ductile shear decreasing structurally upwards towards the Tethyan sedimentary rocks (Fig. 6a). Along the Rongbuk and Kharta valleys, thin leucogranite sills are also present up into the lower-grade rocks below the Qomolangma detachment (Fig. 6b). This suggests that the STD system cuts progressively down-section to the north as shown on the restoration in Figures 2c and 5.

Leucogranites in the GHS are mostly sill complexes intruded parallel to the foliation, with less common late dykes that cross-cut the ductile fabrics, but are truncated by the brittle fault above. Searle *et al.* (2003) defined three major sets of leucogranite sills and dykes, which are broadly comparable across the entire region. These three sets are illustrated from outcrops in the Hermit's Gorge, above the Rongbuk Base camp in Tibet (Fig. 7a,b). Set 1 leucogranites are parallel to the ductile foliation, folded with the metamorphic schistosity and have a weak fabric. Set 2 leucogranite dykes cross-cut the metamorphic fabric, and both sets 1 and 2 are cut by the later set 3 dykes. Set 3 dykes are undeformed garnet + tourmaline + muscovite + biotite leucogranites that cross-cut the ductile fabrics. No leucogranites cut across the brittle STD fault anywhere along the Himalaya, despite earlier reports to the contrary (Manaslu granite (LeFort 1981; Harrison *et al.* 1999), and the Rongbuk granite (Burchfiel *et al.* 1992; Hodges *et al.* 1998)). Along the East Rongbuk glacier the Lhotse detachment truncates foliation in the footwall gneisses (Fig. 8a). The Yellow Band calc-silicates thin towards the north, but form a prominent layer between the high-grade gneiss below and the unmetamorphosed sediments above (Fig. 8b and c). Rocks above the Qomolangma detachment are sedimentary and composed dominantly of calcite with minor amounts of dolomite, quartz and illite-muscovite (Fig. 8d). Rocks beneath the Lhotse detachment show ductile deformation with lower set 1 leucogranite sills folded in with the pelitic and calc-silicate gneisses (Fig. 8e). Structurally higher in the section, flattening fabrics are common with thin leucogranite sills showing boudinage structures (Fig. 8f).

Microstructures within the zone indicate top-to-north kinematics, compatible with extrusion of footwall gneisses to the south beneath a static

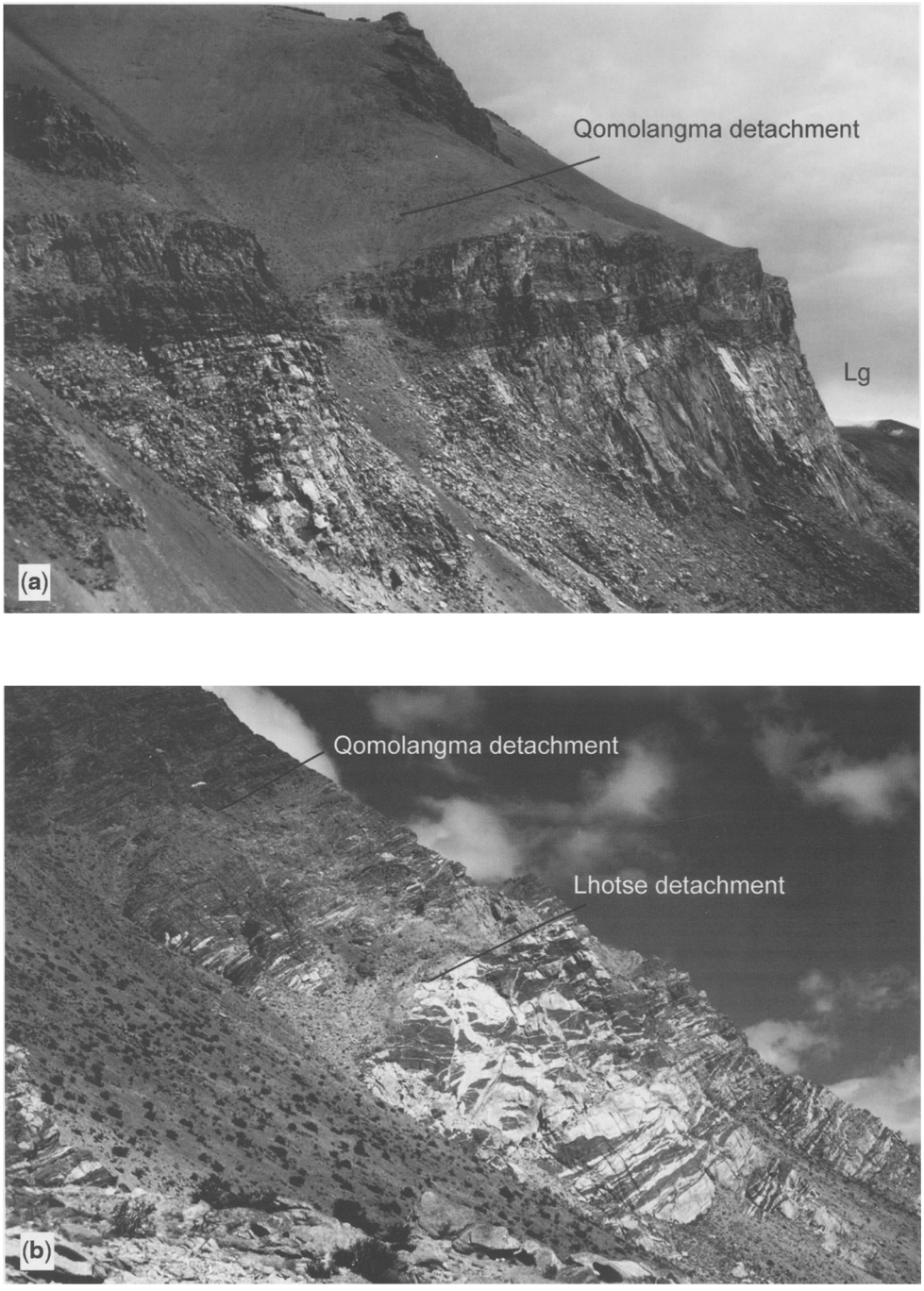


**Fig. 6.** (**a**) Northernmost outcrop of the South Tibetan (STD) along the Rongbuk valley in Tibet, approximately 38 km north of the summit of Everest. Massive cliffs of layered leucogranite (Lg) pass up into ductile deformed gneisses and calc-silicates with fewer leucogranite sills. Metamorphic grade decreases up-section to the Qomolangma Detachment, which places unmetamorphosed limestones and shales above the Greater Himalayan sequence (GHS) metamorphic rocks and leucogranites. (**b**) STD shear zone approximately 60 km north of Everest along the Kharta valley showing upward decrease in volume of leucogranite. The entire section is a large-scale shear zone with ductile strain decreasing upwards towards the base of the Tethyan sedimentary sequence. Cliff section is approximately 80 m high.

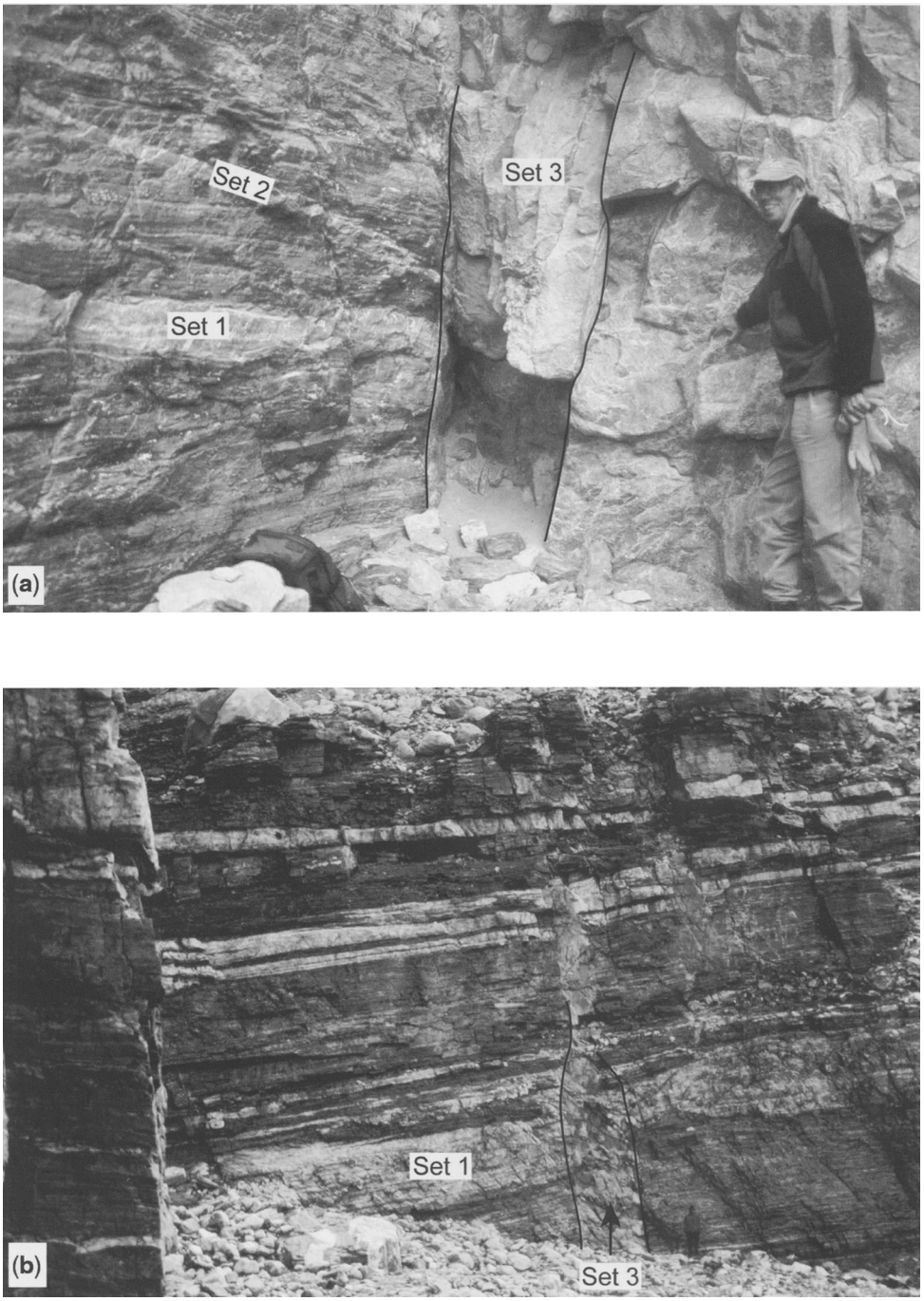


**Fig. 7.** (**a**, **b**) Hermit's Gorge, 5430 m altitude, east of Everest Base camp, Rongbuk glacier. Early, set 1 leucogranite sills are parallel to, and folded in with, the metamorphic schistosity. Set 2 dykes cut the metamorphic schistosity and some of the folds. Both sets 1 and 2 sills and dykes are cut by later, vertical leucogranite dykes (set 3) that abruptly cut folds, metamorphic schistosity and ductile fabric in the gneisses. These late dykes have little or no fabric within, but are cut by the flat-lying brittle Qomolangma Detachment at higher structural levels. Cliff section in (b) is approximately 20 m high.

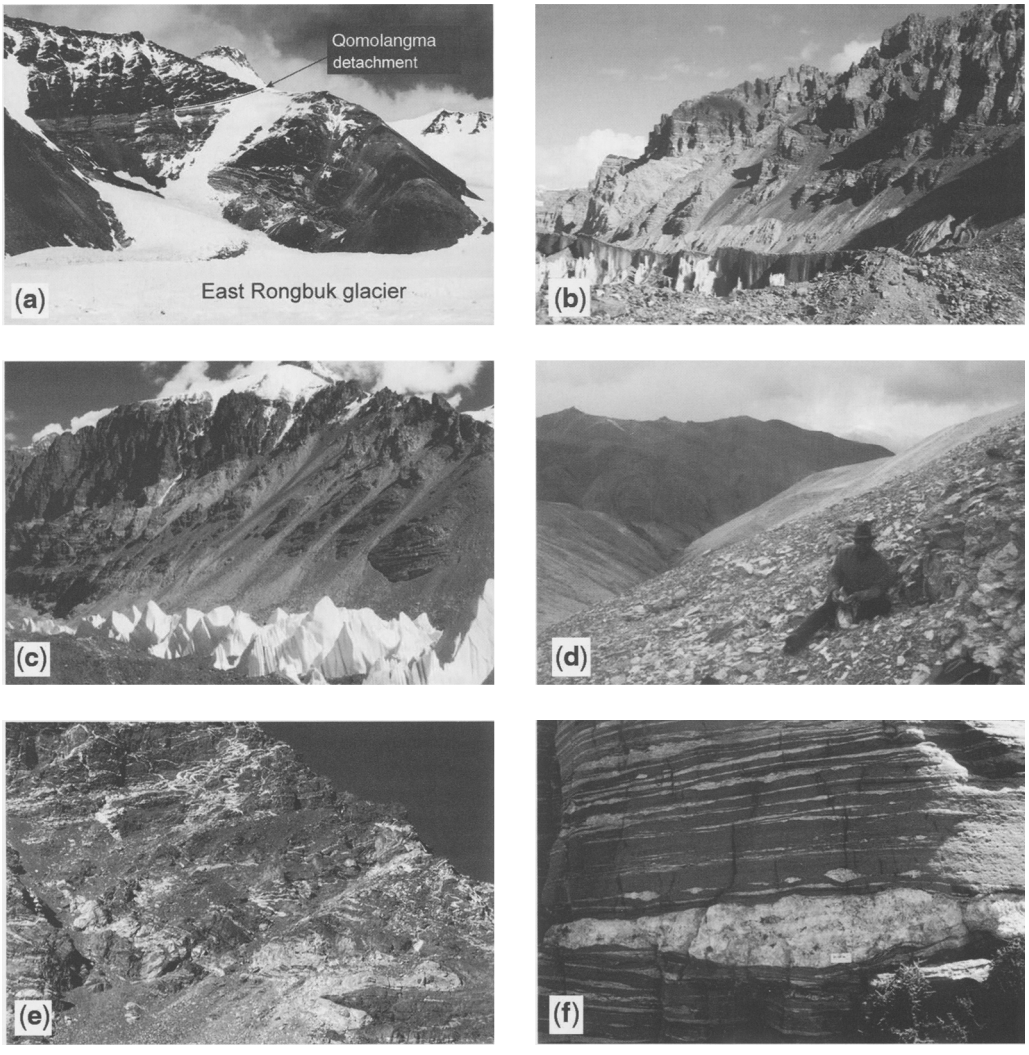


**Fig. 8.** (**a**) Unmetamorphosed Ordovician limestones and mudstones lying above a thin band of calc-silicate (Yellow Band) and high-grade gneisses with leucogranite sills; cliffs east of the East Rongbuk glacier above 6000 m. (**b**) Cliffs of white leucogranite sills intruding gneisses above the East Rongbuk glacier passing up into thin banded calc-silicate and finally into unmetamorphosed sedimentary rocks at top of the cliffs. (**c**) Cliff section above ice penitents of the East Rongbuk glacier. Unmetamorphosed Ordovician sedimentary rocks at the top overlie layered calc-silicates and leucogranite sills below. (**d**) Highest level of the Qomolangma Detachment at *c*. 6000 m above Rongbuk monastery showing the structurally lowest outcrop of sedimentary rocks. (**e**) Folded set 1 leucogranite sills with pelites and calc-silicate gneisses immediately above Rongbuk Base Camp site. (**f**) Flattening boudinage structures in leucogranite sills within the upper level of the Greater Himalayan sequence (GHS) beneath the Lhotse Detachment, lower Rongbuk valley.

hanging wall. Kinematics, vorticity and restoration of the GHS (Searle *et al.* 2002, 2003; Law *et al.* 2004; Jessup *et al.* 2006) show that the STD acted as a 'passive roof fault' (cf. Banks & Warburton 1986), or a 'stretching fault' in the sense of Means (1989). The footwall rocks were extruded out to the south beneath the fault, whilst the hanging wall rocks remained static. Using pressure–depth constraints from footwall gneisses and leucogranites, Walker *et al.* (1999) estimated at least 50 km of southward extrusion of GHS rocks in Zanskar, and Searle *et al.* (2002, 2003)

estimated at least 100 km of southward motion may have occurred in the footwall GHS rocks along the Rongbuk valley, north of Everest. This supports the channel flow model of ductile extrusion of the middle crust. Geochronology suggests that localized partial melting may have triggered channel flow, and that the rapid cooling of the entire GHS slab may have caused channel flow to end abruptly at around 16–14 Ma (Godin *et al.* 2006*a*). $^{40}Ar/^{39}Ar$ muscovite ages, interpreted as a proxy for timing of the ductile to brittle transition, across the entire slab also lend support to this. It is possible, however, that the GHS channel may still be active to the north, at depth beneath south Tibet, and the rocks along the High Himalaya record the 20–16 Ma palaeo-channel.

## Timescales of metamorphism, melting and channel flow

Figure 9 shows geochronological data for the Everest transect plotted on a temperature versus time diagram, with the known closure temperatures for individual minerals in each system on the right. U–Pb dating of monazites growing in equilibrium with garnet, kyanite and sillimanite–cordierite shows that peak metamorphism spanned at least 14 million years, from 32.2 ± 0.4 Ma to 17.9 ± 0.5 Ma (Simpson *et al.* 2000; Searle *et al.* 2003). Large-scale melting to form the Everest leucogranites occurred between 21.3 and 20.5 Ma (Simpson *et al.* 2000) corresponding to the timing of peak high-temperature sillimanite–cordierite-grade metamorphism along the top of the GHS slab. Rapid cooling, and therefore rapid exhumation and probably a period of high erosion rates, followed immediately after crustal melting.

If crustal thickening and regional metamorphism started soon after the India–Asia collision at *c.* 50 Ma then approximately 15–20 million years were required to thicken the crust and metamorphose it to kyanite–sillimanite-grade P–T conditions. Temperatures within the GHS slab must then have remained very high for at least 16 million years (from 32 to 16 Ma), with sporadic episodes of

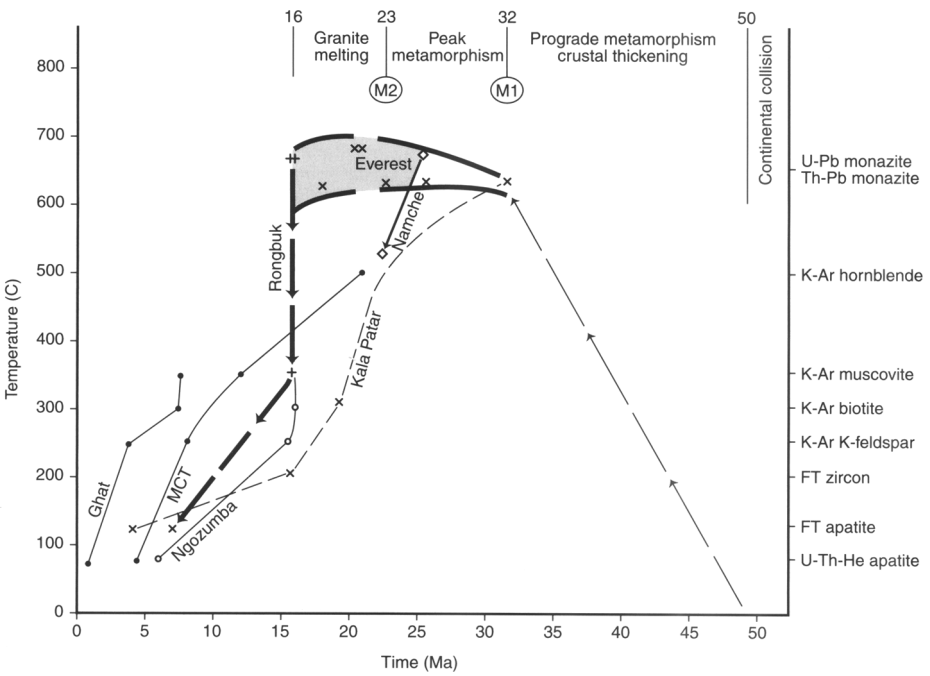


**Fig. 9.** Temperature–time plot showing all geochronological data from the Everest region. Closure temperatures of individual minerals in various isotopic systems are shown on the right-hand side. Monazite ages are interpreted as timing the growth of metamorphic assemblages at or close to the peak, and in granites as timing the crystallization of the granite. Sources of data are Hubbard & Harrison (1989), Bergman *et al.* (1993), Hodges *et al.* (1998), Murphy & Harrison (1999), Hubbard & House (2000), Simpson *et al.* (2000) and Searle *et al.* (2003). The steep part of the cooling path at *c.* 16 Ma is interpreted as the timing of rapid motion of STD footwall rocks as they were exhumed towards the surface.

crustal melting resulting in partial anatexis of the Namche migmatite at 25 Ma (Viskupic & Hodges 2001), and the main pulse of crustal melting forming the Everest–Nuptse–Makalu leucogranites at 21 Ma (Simpson *et al.* 2000). Temperatures within the slab remained high enough for leucogranite generation until 16 Ma when the youngest granite dykes were formed in the Rongbuk area (Murphy & Harrison 1999). All $^{40}Ar/^{39}Ar$ and K–Ar muscovite and biotite ages of GHS metamorphic rocks are older than 14 Ma, suggesting that by that time, the entire GHS slab had cooled to below 350–300°C as the channel cooled, ductile strain had turned to brittle faulting, and thrusting propagated down-structural-section into the Lesser Himalaya.

The timing of metamorphism and melting in the Everest transect closely matches other profiles along the Himalayan chain. In Zanskar, the GHS was metamorphosed to kyanite grade at 33–31 Ma as evidenced by Sm–Nd dating of garnet (Vance & Harris 1999) and U–Pb dating of metamorphic monazite (Walker *et al.* 1999). Temperatures remained high during active crustal shortening and thickening for at least a further 12 million years until 22–20 Ma, when peak sillimanite-grade metamorphism across the GHS slab was coincident with widespread migmatization and crustal melting producing tourmaline, garnet and muscovite-bearing leucogranites (Noble & Searle 1995; Dezes *et al.* 1999; Walker *et al.* 1999). Protoliths of the GHS metamorphic rocks are Proterozoic to early Mesozoic sediments and Permian volcanic rocks (Panjal Traps), partly lateral equivalents to the unmetamorphosed rocks in the Tethyan zone to the north (Searle 1986; Walker *et al.* 2001).

Th–Pb monazite ages within the sillimanite-grade gneisses of the GHS from Pheriche south to Lukla in the Everest transect (Fig. 4) are all within the range 25.3–20.7 Ma (Catlos *et al.* 2002). Only in the far south around the village of Karikhola do the Th–Pb monazite ages become younger, from 15.2 to 11.8 Ma. The monazites are inclusions within garnet that was apparently growing at 530 ± 50°C (Catlos *et al.* 2002), a temperature similar to that required for monazite growth in pelite (525°C; Smith & Barreiro 1990). Catlos *et al.* (2002), following Harrison *et al.* (1997), interpreted these ages as representing late Miocene reactivation of the MCT. Even younger Th–Pb monazite ages (*c.* 7–3 Ma) have been dated in rocks from a similar position along the MCT in central Nepal and Garhwal (Harrison *et al.* 1997; Catlos *et al.* 2002).

Young Th–Pb monazite ages from the MCT present a conundrum for interpreting the tectonic evolution of the MCT. $^{40}Ar/^{39}Ar$ hornblende ages of *c.* 21 Ma from the upper part of the MCT zone south of Lukla, record the timing of cooling through the 500°C isotherm (Hubbard & Harrison 1989). Along most of the Greater Himalaya, $^{40}Ar/^{39}Ar$ and K–Ar muscovite and biotite ages, which record timing of cooling through 300–350°C isotherms, are always older than 14 Ma across the entire slab (Godin *et al.* 2001). How is it possible, therefore, that 530°C metamorphic temperatures in the MCT samples with young monazite ages do not reset the $^{40}Ar/^{39}Ar$ and K–Ar systematics? Recent studies have shown that monazite and even zircon are not only mobile, but can crystallize at temperatures below 350°C in slates (Rasmussen *et al.* 2001; Dempster *et al.* 2004). Rubin *et al.* (1993) showed that zirconium can be a mobile phase during hydrothermal alteration. Young matrix monazites within the MCT zone could therefore have grown during post-metamorphic hydrothermal alteration, but it is harder to explain the monazite inclusions within armouring garnet, unless minute cracks in the garnet allowed access of fluids during hydrothermal activity. The MCT zone has been, and still is, a conduit for boiling fluids, with numerous hot springs located along the thrust (the location of many villages called Tatopani – Nepali for 'hot water'). If the young monazite ages along the MCT zone do record a period of elevated temperatures, it is a very restricted metamorphism solely along the MCT and has no record higher up throughout most of the GHS. The Th–Pb monazite ages south of Kharikhola span 15.2–11.8 Ma (Catlos *et al.* 2002) and may indicate the youngest period of garnet growth in the Phaplu gneiss, immediately prior to cooling below the ductile–brittle transition.

## Discussion

In the channel flow model (Fig. 3) for the Himalaya and Tibet, hot, weak, partially molten and thickened crust flows from the Tibetan plateau towards the plateau margins in response to lithostatic pressure gradients between the high elevation and thick crust of Tibet and the low elevation and normal thickness of the Indian plate crust. Channel flow processes have been incorporated into both linear viscous models and coupled thermal–mechanical models (Royden *et al.* 1997; Beaumont *et al.*, 2001, 2004). Previously, the deformation has been thought of in terms of a 'jelly sandwich' model in which the upper crust and upper mantle are strong, and are separated by a weak and ductile lower crust (Jackson *et al.* 2004). However, in the Himalaya it is the middle crust that is hot, weak and flowing, whereas the

granulitic lower (Indian) crust is relatively strong. The lower crust of Tibet is not exposed so we have to rely on gravity data (Jin *et al.* 1994), seismic data (Nelson *et al.* 1996) and volcanic xenoliths (Hacker *et al.* 2000) to interpret the structure.

The INDEPTH seismic experiments in southern Tibet indicate the presence of a fluid-like layer of middle crust (Nelson *et al.* 1996; Brown *et al.* 1996) interpreted as containing a degree of partial melt. This mid-crust layer can be followed south to link with the GHS and the bounding shear zones of the MCT and STD. We suggest that the crust beneath the Himalaya and southern Tibet must be rheologically layered, with a major decoupling of the upper, middle and lower crust (Fig. 10). The geotherm is not linear with depth but shows a peak temperature at high levels in the middle crust, corresponding to the location of the 'bright spots' imaged by magnetotelluric data beneath the Lhasa block (Kola-Ojo & Meissner 2001). The lower crust is composed of the more rigid, dry granulites of the underthrusting Indian shield. Earthquakes in southern Tibet are abundant in the upper crust down to *c.* 18 km and again in the lowermost crust at 60–80 km, but not in the middle crust (Jackson *et al.* 2004), in agreement with the non-linear isotherm shown in Figure 10. There is however, some dispute as to whether the deep earthquakes beneath the Himalaya and south Tibet are actually in the lower crust or in the upper mantle (Chen & Yang 2004).

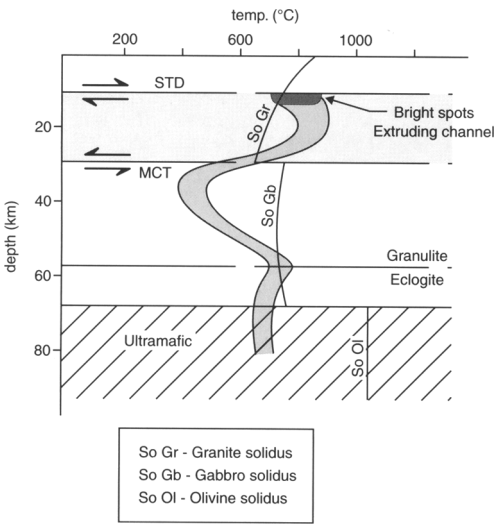


**Fig. 10.** Proposed geotherm beneath the southern part of the Tibetan plateau, using structural depths and temperatures from the Everest transect across the Greater Himalayan sequence (GHS) (Hubbard 1996; Searle *et al.* 2003) as a reverse uniformitarian analogue (Miocene P–T profile across the GHS is used as a guide to the present temperature–depth profile beneath the plateau). The positions of the 'bright spots' and temperatures in the lower crust and upper mantle are after Kola-Ojo & Meissner (2001). The mid-crustal channel, bounded by the Main Central Thrust (MCT) below and the South Tibetan detachment (STD) above, is shaded with the location of the 'bright spots' imaged on the INDEPTH deep seismic profile, and interpreted as leucogranite magmas forming today, also shown. The lower crust, between about 35 and 75 km, is composed of Indian shield granulites underthrust beneath the southern margin of the Lhasa block.

The obvious question now is why do melting temperatures exist at relatively shallow levels of the thick crust beneath the south Tibetan plateau? The restoration of the Everest transect (Fig. 5) shows that the leucogranites were derived from the Proterozoic shales along a stratigraphic horizon that must have formed the protolith of the migmatites and leucogranites. The heat source for melting cannot have been frictional heating along the MCT because the site of anatexis is along much higher crustal levels than the MCT, and *in situ* melting is not seen along the MCT. We suggest that the shallow level of high temperatures producing leucogranite melts must have been the consequence of a high concentration of radioactive heat-producing elements at that unique stratigraphic horizon in the crust. The concentration of U, Th and K could have been the result of sedimentary processes within the late Proterozoic basin that accumulated debris off the eroding Archaean mountain belt of peninsula India.

Another intriguing question remaining is: why did channel flow operate within a relatively narrow time span (24–17 Ma), and why did it apparently end at *c.* 16 Ma? High temperatures, close to leucogranite melting temperatures (680–720°C), are required to maintain ductile channel flow. Numerous $^{40}Ar/^{39}Ar$ and K–Ar cooling ages on micas within the GHS are almost entirely older than 15–14 Ma (see Searle & Godin (2003) and Godin *et al.* (2006*a*,*b*) for a summary). Temperatures in the GHS metamorphic rocks and leucogranites must therefore have been below 350°C by 15–14 Ma, and the whole channel must have cooled through the ductile–brittle transition. This fact makes the subsequent late Miocene–Pliocene monazite ages from the MCT zone (Harrison *et al.* 1997; Catlos *et al.* 2002) hard to interpret as indicators of a regional metamorphic event.

It is possible that the Himalayan mid-crustal channel could still be active today (Hodges *et al.* 2001), although there is no seismic evidence for recent activity on the MCT or the STD. The GHS along the High Himalaya corresponds to the zone of highest topography, although some of the highest peaks along the range (e.g. Dhaulagiri–Annapurna

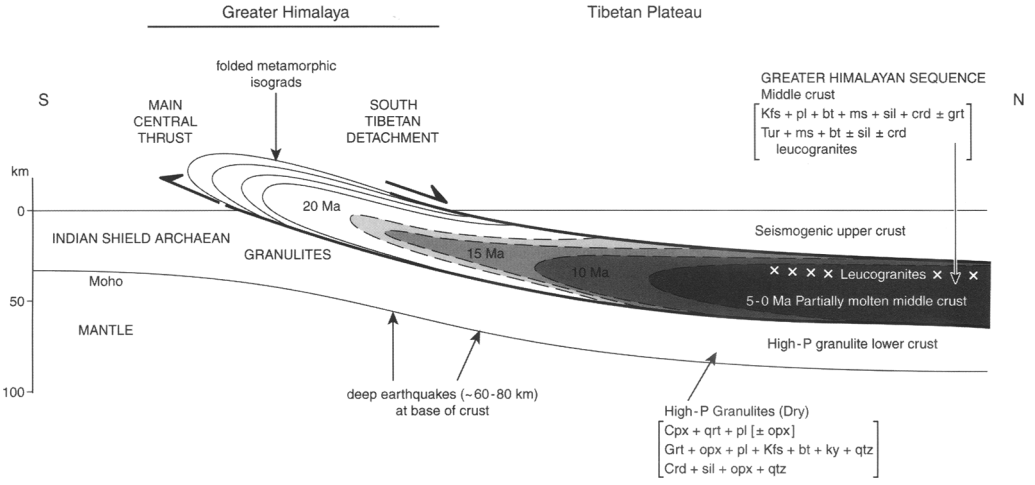


**Fig. 11.** Sketch section across the Himalaya and south Tibet showing how the channel flow model could work if channel flow was operating today. The folded metamorphic isograds linking the STD footwall and MCT hanging wall represent 'frozen' 20–15 Ma isograds adjacent to a younger and more active channel of partial melting present beneath southern Tibet today. This partially molten mid-crustal channel separates the seismogenic upper crust, dominated today by east–west extension, and the granulite facies lower crust dominated by north–south compression. Indian Shield granulites subducted to 50–75 km depth beneath south Tibet would remain at granulite facies unless hydrated, in which case they would convert to eclogite facies rocks. The deepest earthquakes occur along the base of the crust as it flexes down beneath the Himalaya.

peaks) are composed of the lower Tethyan sedimentary rocks above the STD. Hurtado *et al.* (2001) suggested that one branch of the STD north of Annapurna may have been active during the Quaternary. The MCT is coincident with prominent knick-points in Himalayan river profiles (Seeber & Gornitz 1983), but the hanging wall uplift could be due either to MCT reactivation (Harrison *et al.* 1997, 1998) or to uplift above a ramp along the deeper and younger Main Himalayan thrust (MHT) fault (Cattin & Avouac 2000). If the high topography of the Himalaya is due to channel flow during the period 24–16 Ma, why does the range remain so high today? One solution would be to have the Miocene channel preserved along the Himalaya today, as recorded by the geological structure and pressure–temperature–time conditions, as an outer rind or crust surrounding the hot, active channel presently at mid-crustal depths beneath the southern part of the Tibetan plateau (Fig. 11). This could be envisaged as analogous to a cooling Hawaiian-type lava flow with a hot, molten core surrounded by a cooling brittle carapace.

## Conclusions

Field mapping, macro- and micro-structural observations, and thermal modelling all support the conclusion that the channel flow model is appropriate for the GHS. A slab of Indian plate middle crust, between 5 and 20 km thick, was at fairly uniform high temperatures (*c.* 600–700°C) for a period of about 12–16 million years during the late Oligocene and early Miocene (between 30 and 17 Ma), sandwiched between a brittle-deforming upper crust (Tethyan sedimentary zone) and a rigid granulitic lower crust (subducting Indian shield). The mid-crustal channel was metamorphosed at sillimanite-grade temperatures and contained a zone of *in situ* early Miocene migmatization, up to 5–8 km thick. The GHS channel was bounded by two major ductile shear zones with thrust sense of shear along the base (MCT), and a normal sense of shear above (STD).

Structural geometry, thermobarometry and geochronology suggest that there was a mid-crustal layer composed of high-temperature sillimanite-grade rocks that were close to partial melting temperatures during the period 32–17 Ma. Migmatites and crustal melt leucogranites are widespread at the upper structural levels of this layer. U–Pb dating of metamorphic monazites crystallizing in equilibrium with garnet and kyanite, indicates that early metamorphism in the Everest area peaked at 32.2 $\pm$ 0.4 Ma (Simpson *et al.* 2000). Similar ages were obtained from Sm–Nd dating of garnets in the Zanskar and Garhwal regions in the western Himalaya (Vance & Harris 1999;

Prince *et al.* 2001). It appears that, although high temperatures were attained by 32 Ma, melting did not occur along the top of the GHS until about 24–21 Ma, at least in the Everest–Makalu region (Schärer 1984; Simpson *et al.* 2000). These ages suggest that it could have been partial melting that triggered channel flow and ductile extrusion. The timing of granite melting also coincides with the timing of increased cooling rates, erosion rates and exhumation of the GHS, and increased sedimentation rates in the Siwalik foreland basin. As the granites cooled, flow ended and lateral transport was achieved by brittle faulting along the outer margins of the channel, both below (MCT) and above (STD).

Melting resulted in several large leucogranite bodies that reach a maximum thickness of *c.* 3 km in the Makalu–Chomolonzo leucogranite body. Himalayan leucogranites contain tourmaline, garnet, muscovite and biotite and are pure crustal melts, derived from a highly radiogenic Proterozoic sedimentary source, corresponding to the Haimanta Group shales (or Cheka Group in Bhutan). The shallow level of crustal melting within the Himalayan crust must have been the result of a high concentration of heat-producing elements within the stratigraphic horizon of the Proterozoic black shales. The Himalayan granites were intruded as sill complexes within the sillimanite gneisses for large distances (over 70–100 km north of Everest) laterally along the foliation planes.

Microstructures within the GHS channel indicate that there was a significant component of penetrative vertical pure shear, as well as the dominant south-directed simple shear (Law *et al.* 2004; Jessup *et al.* 2006). However, despite the evidence for a reduction in the thickness of the channel through flattening, there is also good evidence that the active channel expanded with time, during a change from ductile to brittle deformation, as MCT zone thrusts propagated down-structural-section with time, and STD normal faults propagated up-section with time. Thrust faults along the base of the channel and normal faults along the top must have been synchronous, as previously suggested (Searle & Rex 1989; Hodges *et al.* 1993, 1996; Searle *et al.* 1997, 2003).

STD normal faults were active in a wholly compressional environment, and acted as a passive roof fault during crustal shortening and thickening in the footwall. Although pure shear flattening did compress the sequence, new material was constantly being fed into the channel from crustal subduction beneath the active MCT during the late Oligocene and Miocene. Folding and thrusting in the Tethyan sedimentary rocks above the STD occurred earlier than shortening and thickening in the GHS beneath, although some breakback thrusting and north-directed backthrusting did occur late in the sequence (Searle 1986; Corfield & Searle 2000; Murphy & Yin 2003). The STD normal faults do not relate to wholescale crustal thinning, whole crustal extension or topographic collapse.

This work was funded by NERC grant NER/K/S/2000/0951 to M.P.S and NSF grant EAR 0207524 to R.D.L. We are grateful to Randy Parrish, Dave Waters and Rob Simpson for extensive discussions, and to Brad Hacker and Mike Murphy for reviews. We also are very grateful to Tashi Sherpa, Ting Lei, Sonan Wangdu, Rene Schrama and Shiva Dhaktal for logistics. This paper is dedicated to Doug Nelson in memory of his enthusiastic and scholarly input into tapping the mysteries of Tibetan structure, and for breaching the geology–geophysics mental barrier.

## References

ALSDORF, D. & NELSON, K. D. 1999. Tibetan satellite magnetic low: Evidence for widespread melt in the Tibetan crust? *Geology*, **27**, 943–946.

ALSDORF, D., BROWN, L., NELSON, K. D., MAKOVSKY, Y., KLEMPERER, S. & ZHAO, W. 1998. Crustal deformation of the Lhasa terrane from Project INDEPTH deep seismic reflection profiles. *Tectonics*, **17**, 501–519.

ARITA, K. 1983. Origin of the inverted metamorphism of the lower Himalaya, central Himalaya. *Tectonophysics*, **95**, 43–60.

BANKS, C. J. & WARBURTON, J. 1986. 'Passive-roof' duplex geometry in the frontal structures of the Kirthar and Sulaiman mountain belts, Pakistan. *Journal of Structural Geology*, **8**, 229–237.

BEAUMONT, C., JAMIESON, R. A., NGUYEN, M. H. & LEE, B. 2001. Himalayan tectonics explained by extrusion of a low-viscosity crustal channel coupled to focused surface denudation. *Nature*, **414**, 738–742.

BEAUMONT, C., JAMIESON, R. A., NGUYEN, M. H. & MEDVEDEV, S. 2004. Crustal channel flows: 1. Numerical models with applications to the tectonics of the Himalayan–Tibetan orogen. *Journal of Geophysical Research*, **109**, B06406.

BERGMAN, S. C., COFFIELD, D. Q., DONELICK, R., CORRIGAN, J., TALBOT, J., CERVENY, P. & KELLEY, S. 1993. Late Cenozoic compressional and extensional cooling and exhumation of the Qomolangma (Mt. Everest) region, Nepal. *Geological Society of America Abstracts with Programs*, **25**(6), A-176 (abstract).

BIRD, P. 1991. Lateral extrusion of lower crust from under high topography, in the isostatic limit. *Journal of Geophysical Research*, **96**, 10,275–10,286.

BROWN, L. D., ZHAO, W., NELSON, K. D. *ET AL.* 1996. Bright spots, structure and magmatism in Southern Tibet from INDEPTH seismic reflection profiling. *Science*, **274**, 1688–1690.

BURCHFIEL, B. C., ZHILIANG, C., HODGES, K. V., YUPING, L., ROYDEN, L., CHANGRONG, D. & JIENE, X. 1992. *The South Tibetan Detachment System, Himalayan Orogen: extension contemporaneous with and parallel to shortening in a collisional mountain belt*. Geological Society of America, Special Paper, **269**.

BURG, J.-P. 1983. *Carte Géologique du Sud du Tibet*. Ministry of Geology, Peking, and CNRS, Paris.

BURG, J. P., BRUNEL, M., GAPAIS, D., CHEN, G. M. & LIU, G. H. 1984. Deformation of leucogranites of the crystalline Main Central thrust sheet in southern Tibet (China). *Journal of Structural Geology*, **6**, 535–542.

CAROSI, R., LOMBARDO, B., MOLLI, G., MUSUMECI, G. & PERTUSATI, P. 1998. The South Tibetan detachment system in the Rongbuk valley, Everest region. Deformation features and geological implications. *Journal of Asian Earth Sciences*, **16**, 299–311.

CAROSI, R., LOMBARDO, B., MUSUMECI, G. & PERTUSATI, P. 1999*a*. Geology of the Higher Himalayan crystallines in Khumbu Himal (Eastern Nepal). *Journal of Asian Earth Sciences*, **17**, 785–803.

CAROSI, R., MUSUMECI, G. & PERTUSATI, P. C. 1999*b*. Extensional tectonics in the higher Himalayan crystallines of Khumbu Himal, eastern Nepal. *Geological Society of America Special Paper* **328**, 211–223.

CATLOS, E. J., HARRISON, T. M., MANNING, C. E., GROVE, M., RAI, S. M., HUBBARD, M. & UPRETI, B. N. 2002. Records of the evolution of the Himalayan orogen from in situ Th-Pb ion microprobe dating of monazite: Eastern Nepal and western Garhwal. *Journal of Asian Earth Sciences*, **20**, 459–480.

CATTIN, R. & AVOUAC, J.-P. 2000. Modeling mountain building and the seismic cycle in the Himalaya of Nepal. *Journal of Geophysical Research*, **105**, 13,389–13,407.

CHEN, W.-P. & YANG, Z. 2004. Earthquakes beneath the Himalaya and Tibet: Evidence for strong lithospheric mantle. *Science*, **304**, 1949–1952.

CLARK, M. K. & ROYDEN, L. H. 2000. Topographic ooze: Building the eastern margin of Tibet by lower crustal flow. *Geology*, **28**, 703–706.

COLCHEN, M., LE FORT, P. & PECHER, A. 1986. *Annapurna–Manaslu–Ganesh Himal*. CNRS, Paris.

CORFIELD, R. I. & SEARLE, M. P. 2000. Crustal shortening estimates across the north Indian continental margin, Ladakh, NW India. *In*: KHAN, M. A., TRELOAR, P. J., SEARLE, M. P. & JAN, M. Q. (eds) *Tectonics of the Nanga Parbat Syntaxis and the Western Himalaya*. Geological Society, London, Special Publications, **170**, 395–410.

DECELLES P. G., GEHRELS, G. E., QUADE, J., LAREAU, B. & SPURLIN, M. 2000. Tectonic implications of U-Pb zircon ages of the Himalayan orogenic belt in Nepal. *Science*, **288**, 497–499.

DEMPSTER, T. J., HAY, D. & BLUCK, B. J. 2004. Zircon growth in slate. *Geology*, **32**, 221–224.

DEZES, P. J., VANNAY, J.-C., STECK, A., BUSSY, F. & COSCA, M. 1999. Synorogenic extension: Quantitative constraints on the age and displacement of the Zanskar shear zone (northwest Himalaya). *Geological Society of America Bulletin*, **111**, 364–374.

DUCEA, M. N., LUTKOV, V., MINAEV, V. T. *ET AL.* 2003. Building the Pamirs: The view from the underside. *Geology*, **31**, 849–852.

DUNCAN, C., MASEK, J. & FIELDING, E. 2003. How steep are the Himalaya? Characteristics and implications of along-strike topographic variations. *Geology*, **31**, 75–78.

FIELDING, E., ISACKS, B., BARAZANGI, M. & DUNCAN, C. 1994. How flat is Tibet? *Geology*, **22**, 163–167.

FRANCHETEAU, J., JAUPART, C., XIAN, J. S. *ET AL.* 1984. High heat flow in southern Tibet. *Nature*, **307**, 32–36.

GAILLARD, F., SCAILLET, B. & PICHAVANT, M. 2004. Evidence of present-day leucogranite pluton growth in Tibet. *Geology*, **32**, 801–804.

GANSSER, A. 1964. *Geology of the Himalaya*. John Wiley & Sons, Chichester.

GANSSER, A. 1983. *Geology of the Bhutan Himalaya*. Birkhäuser Verlag, Basle.

GODIN, L., PARRISH, R. R., BROWN, R. D. & HODGES, K. V. 2001. Crustal thickening leading to exhumation of the Himalayan core of central Nepal: insights from U-Pb geochronology and $^{40}Ar/^{39}Ar$ thermochronology. *Tectonics*, **20**, 729–747.

GODIN, L., GRUJIC, D., LAW, R. D. & SEARLE, M. P. 2006*a*. Channel flow, extrusion and exhumation in continental collision zones: an introduction. *In*: LAW, R. D., SEARLE, M. P. & GODIN, L. (eds) *Channel Flow, Ductile Extrusion and Exhumation in Continental Collision Zones*. Geological Society, London, Special Publications, **268**, 1–23.

GODIN, L., GLEESON, T., SEARLE, M. P., ULLRICH, T. D. & PARRISH, R. R. 2006*b*. Locking of southward extrusion in favour of rapid crustal-scale buckling of the Greater Himalayan sequence, Nar valley, central Nepal. *In*: LAW, R. D., SEARLE, M. P. & GODIN, L. (eds) *Channel Flow, Ductile Extrusion and Exhumation in Continental Collision Zones*. Geological Society London, Special Publications, **268**, 269–292.

GRASEMANN, B., FRITZ, H. & VANNAY, J.-C. 1999. Quantitative kinematic flow analysis from the Main Central Thrust zone, (NW Himalaya): implications for a decelerating strain path and the extrusion of orogenic wedges. *Journal of Structural Geology*, **21**, 837–853.

GRUJIC, D., CASEY, M., DAVIDSON, C., HOLLISTER, L., KUNDIG, K., PAVLIS, T. & SCHMID, S. 1996. Ductile extrusion of the Higher Himalayan crystalline in Bhutan: evidence from quartz microfabrics. *Tectonophysics*, **260**, 21–43.

GRUJIC, D., HOLLISTER, L. & PARRISH, R. R. 2002. Himalayan metamorphic sequence as an orogenic channel: insight from Bhutan. *Earth and Planetary Science Letters*, **198**, 177–191.

HACKER, B. R., GNOS, E., RATSCHBACHER, L. *ET AL.* 2000. Hot and dry deep crustal xenoliths from Tibet. *Science*, **287**, 2463–2466.

HARRISON, T. M., RYERSON, F. J., LE FORT, P., YIN, A., LOVERA, O. & CATLOS, E. J. 1997. A Late Miocene–Pliocene origin for the central Himalayan inverted metamorphism. *Earth and Planetary Science Letters*, **146**, E1–E8.

HARRISON, T. M., GROVE, M., LOVERA, O. & CATLOS, E. J. 1998. A model for the origin of Himalayan anatexis and inverted metamorphism. *Journal of Geophysical Research*, **103**, 27,017–27,032.

HARRISON, T. M., GROVE, M., MCKEEGAN, K. D., COATH, C. D., LOVERA, O. & LEFORT, P. 1999. Origin and episodic emplacement of the Manaslu Intrusive Complex, Central Himalaya. *Journal of Petrology*, **40**, 3–19.

HAUCK, M. L., NELSON, K. D., BROWN, L. D., ZHAO, W. & ROSS, A. R. 1998. Crustal structure of the Himalayan orogen at approximately 90° east longitude from Project INDEPTH deep reflection profiles. *Tectonics*, **17**, 481–500.

HODGES, K. V. 2000. Tectonics of the Himalaya and southern Tibet from two perspectives. *Geological Society of America Bulletin*, **112**, 324–350.

HODGES, K. V., PARRISH, R. R., HOUSCH, T. B., LUX, D. R., BURCHFIEL, B. C., ROYDEN, L. H. & CHEN, Z. 1992. Simultaneous Miocene extension and shortening in the Himalayan orogen. *Science*, **258**, 1466–1470.

HODGES, K. V., BURCHFIEL, B. C., ROYDEN, L. H., CHEN, Z. & LIU, Y. 1993. The metamorphic signature of contemporaneous extension and shortening in the central Himalayan orogen: data from the Nyalam transect, southern Tibet. *Journal of Metamorphic Geology*, **11**, 721–737.

HODGES, K. V., PARRISH, R. R. & SEARLE, M. P. 1996. Tectonic evolution of the central Annapurna Range, Nepalese Himalaya. *Tectonics*, **15**, 1264–1291.

HODGES, K. V., BOWRING, S., DAVIDEK, K., HAWKINS, D. & KROL, M. 1998. Evidence for rapid displacement on Himalayan normal faults and the importance of tectonic denudation in the evolution of mountain ranges. *Geology*, **26**, 483–486.

HODGES, K. V., HURTADO, J. M. & WHIPPLE, K. X. 2001. Southward extrusion of Tibetan crust and its effect on Himalayan tectonics. *Tectonics*, **20**, 799–809.

HUBBARD, M. S. 1989. Thermobarometric constraints on the thermal history of the Main Central Thrust Zone and Tibetan Slab, eastern Nepal Himalaya. *Journal of Metamorphic Geology*, **7**, 19–30.

HUBBARD, M. S. 1996. Ductile shear as a cause of inverted metamorphism: Example from the Nepal Himalaya. *Journal of Geology*, **194**, 493–499.

HUBBARD, M. S. & HARRISON, T. M. 1989. $^{40}Ar/^{39}Ar$ age constraints on deformation and metamorphism in the Main Central Thrust zone and Tibetan Slab, eastern Nepal Himalaya. *Tectonics*, **8**, 865–880.

HUBBARD, M. S. & HOUSE, M. 2000. Low temperature dating of high mountain rocks: (U-Th)/He ages from Higher Himalayan samples, Eastern Nepal. *Earth Sciences Frontiers, Beijing, 15th Himalaya–Karakoram–Tibet Workshop, Chengdu*, 16–17, (abstract).

HURTADO, J. M., HODGES, K. V. & WHIPPLE, K. X. 2001. Neotectonics of the Thakkhola graben and implications for recent activity on the South Tibetan Fault system in the central Nepalese Himalaya. *Geological Society of America Bulletin*, **113**, 222–240.

JACKSON, J., AUSTRHEIM, H., MCKENZIE, D. & PREISTLEY, K. 2004. Metastability, mechanical strength, and the support of mountain belts. *Geology*, **32**, 625–628.

JAMIESON, R. A., BEAUMONT, C., MEDVEDEV & NGUYEN, M. H. 2004. Crustal channel flows: 2. Numerical models with implications for metamorphism in the Himalayan-Tibetan orogen. *Journal of Geophysical Research*, **109**, B06407.

JESSUP, M. J., TRACY, R., SEARLE, M. P. & LAW, R. D. 2004. Staurolite schist marks right-way up metamorphic isograds at the top of the High Himalayan Slab: Mount Everest, Tibet/Nepal. *In*: SEARLE, M. P., LAW, R. D. GODIN, L. (convenors) *Channel Flow, Ductile Extrusion and Exhumation of Lower-mid Crust in Continental Collision Zones*, *Abstract Books*, Geological Society, London.

JESSUP, M. J., LAW, R. D., SEARLE, M. P. & HUBBARD, M. S. 2006. Structural evolution and vorticity of flow during extrusion and exhumation of the Greater Himalayan Slab, Mount Everest Massif, Tibet/Nepal: implications for orogen-scale flow partitioning. *In*: LAW, R. D., SEARLE, M. P. & GODIN, L. (eds) *Channel Flow, Ductile Extrusion and Exhumation in Continental Collision Zones*. Geological Society, London, Special Publications, **268**, 379–413.

JIN, Y., MCNUTT, M. K. & ZHU, Y. 1994, Evidence from gravity and topography data for folding of Tibet. *Nature*, **371**, 669–674.

KIND, R., NI., J., ZHAO, W. *ET AL.* 1996. Evidence from earthquake data for a partially molten crustal layer in southern Tibet. *Science*, **274**, 1692–1694.

KOLA-OJO, O. & MEISSNER, R. 2001. Southern Tibet: its deep seismic structure and some tectonic implications. *Journal of Asian Earth Sciences*, **19**, 249–256.

KOSAREV, G., KIND, R., SOBOLEV, S. V., YUAN, X., HANKA, W. & ORESHIN, S. 1999. Seismic evidence for a detached Indian lithospheric mantle beneath Tibet. *Science*, **283**, 1306–1309.

LAW, R. D., SEARLE, M. P. & SIMPSON, R. L. 2004. Strain, deformation temperatures and vorticity of flow at the top of the Greater Himalayan Slab, Everest massif, Tibet. *Journal of the Geological Society, London*, **161**, 305–320.

LE FORT, P. 1981. Manaslu leucogranite: a collision signature of the Himalaya–a model for its genesis and emplacement. *Journal Geophysical Research*, **86**, 10,545–10,568.

LOMBARDO, B., PERTUSATI, P. & BORGI, S. 1993. Geology and tectonomagmatic evolution of the eastern Himalaya along the Chomolungma - Makalu transect. *In*: TRELOAR, P. J. & SEARLE, M. P. (eds) *Himalayan Tectonics*. Geological

Society, London, Special Publications, **74**, 341–355.

MEANS, W. D. 1989. Stretching faults. *Geology*, **17**, 893–896.

MILLER, C., THONI, M., FRANK, W., GRASEMAN, B., KLOTZLI, U., GUNTLI, P. & DRAGANTIS, E. 2001. The early Palaeozoic magmatic event in the Northwest Himalaya, India: source, tectonic setting and age of emplacement. *Geological Magazine*, **138**, 237–251.

MURPHY, M. A. & HARRISON, T. M. 1999. Relationship between leucogranites and the Qomolangma Detachment in the Rongbuk valley, south Tibet. *Geology*, **27**, 831–834.

MURPHY, M. A. & YIN, A. 2003. Structural evolution and sequence of thrusting in the Tethyan fold-thrust belt and Indus-Yalu suture zone, southwest Tibet. *Geological Society of America Bulletin*, **115**, 21–34.

NELSON, K. D., ZHAO, W. J., BROWN, L. D. *ET AL.* 1996. Partially molten middle crust beneath southern Tibet: synthesis of Project INDEPTH results. *Science*, **274**, 1684–1688.

NOBLE, S. R. & SEARLE, M. P. 1995. Age of crustal melting and leucogranite formation from U-Pb zircon and monazite dating in the western Himalaya, Zanskar, India. *Geology*, **23**, 1135–1138.

OWENS, T. J. & ZANDT, G. 1997. Implications of crustal property variations for models of Tibetan plateau evolution. *Nature*, **387**, 37–43.

PARRISH, R. R. & HODGES, K. V. 1996. Isotopic constraints on the age and provenance of the Lesser and Greater Himalayan sequences, Nepalese Himalaya. *Geological Society of America Bulletin*, **108**, 904–911.

POGNANTE, U. & BENNA, P. 1993. Metamorphic zonation, migmatization and leucogranites along the Everest transect of eastern Nepal and Tibet: record of an exhumation history, *In*: TRELOAR, P. J. & SEARLE, M. P. (eds) *Himalayan Tectonics*. Geological Society, London, Special Publications, **74**, 323–340.

PRINCE, C., HARRIS, N. & VANCE, D. 2001. Fluid-enhanced melting during prograde metamorphism. *Journal of Geological Society, London*, **158**, 233–241.

RASMUSSEN, B., FLETCHER, I. R. & MACNAUGHTON, N. J. 2001. Dating of low grade metamorphic events by SHRIMP U-Pb analysis of monazite in shale. *Geology*, **29**, 963–966.

ROBINSON, D., DECELLES, P. G., GARZIONE, C. N., PEARSON, O. N., HARRISON, T. M. & CATLOS, E. J. 2003. Kinematic model for the Main Central thrust in Nepal. *Geology*, **31**, 359–362.

ROBYR, M., VANNAY, J.-C., EPARD, J.-L. & STECK, A. 2002. Thrusting, extension, and doming during the polyphase tectonometamorphic evolution of the high Himalayan crystalline zone in NW India. *Journal of Asian Earth Sciences*, **21**, 221–239.

ROYDEN, L. H., BURCHFIEL, B. C., KING, R. W., WANG, E., CHEN, Z., SHEN, F. & LIU, Y. 1997. Surface deformation and lower crustal flow in eastern Tibet. *Science*, **276**, 788–790.

RUBIN, J. N., HENRY, C. D. & PRICE, J. G. 1993. The mobility of zirconium and "immobile" elements during hydrothermal alteration. *Chemical Geology*, **110**, 29–47.

SCHARER, U. 1984. The effect of initial $^{230}$Th disequilibration on U-Pb ages: the Makalu case. *Earth and Planetary Science Letters*, **67**, 191–204.

SEARLE, M. P. 1986. Structural evolution and sequence of thrusting in the High Himalaya, Tibetan-Tethys and Indus suture zones of Zanskar and Ladakh, Western Himalaya. *Journal of Structural Geology*, **8**, 923–936.

SEARLE, M. P. 1999*a*. Extensional and compressional faults in the Everest–Lhotse massif, Khumbu Himalaya, Nepal. *Journal of Geological Society, London*, **156**, 227–240.

SEARLE, M. P. 1999*b*. Emplacement of Himalayan leucogranites by magma injection along giant sill complexes: examples from the Cho Oyu, Gyachung Kang and Everest leucogranites (Nepal Himalaya). *Journal of Asian Earth Sciences*, **17**, 773–783.

SEARLE, M. P. 2003. *Geological Map of the Everest Massif, Nepal and South Tibet.* Scale 1:100,000. Department of Earth Sciences, Oxford University.

SEARLE, M. P. & GODIN, L. 2003. The South Tibetan Detachment and the Manaslu Leucogranite: A structural re-interpretation and restoration of the Annapurna – Manaslu Himalaya, Nepal. *Journal of Geology*, **111**, 505–523.

SEARLE, M. P. & REX, A. J. 1989. Thermal model for the Zanskar Himalaya. *Journal of Metamorphic Geology*, **7**, 127–134.

SEARLE, M. P. & SZULC, A. G. 2005. Channel Flow and ductile extrusion of the high Himalayan slab–the Kangchenjunga—Darjeeling profile, Sikkim Himalaya. *Journal of Asian Earth Sciences*, **25**, 173–185.

SEARLE, M. P., WATERS, D. J., REX, D. C. & WILSON, R. N. 1992. Pressure, temperature and time constraints on Himalayan metamorphism from eastern Kashmir and western Zanskar. *Journal of Geological Society, London*, **149**, 753–773.

SEARLE, M. P., METCALFE, R. P., REX, A. J. & NORRY, M. J. 1993. Field relations, petrogenesis and emplacement of the Bhagirathi leucogranite, Garhwal Himalaya. *In*: TRELOAR, P. J. & SEARLE, M. P. (eds) *Himalayan Tectonics*. Geological Society, London, Special Publications, **74**, 429–444.

SEARLE, M. P., PARRISH, R. R., HODGES, K. V., HURFORD, A., AYRES, M. W. & WHITEHOUSE, M. J. 1997. Shisha Pangma leucogranite, South Tibetan Himalaya: Field Relations, geochemistry, age, origin and emplacement, *Journal of Geology*, **105**, 295–317.

SEARLE, M. P., NOBLE, S. R., HURFORD, A. J. & REX, D. C. 1999*a*. Age of crustal melting, emplacement and exhumation history of the Shivling leucogranite, Garhwal Himalaya. *Geological Magazine*, **136**, 513–525.

SEARLE, M. P., WATERS, D. J., DRANSFIELD, M. W., STEPHENSON, B. J., WALKER, C. B., WALKER, J. D. & REX, D. C. 1999*b*. Thermal and mechanical models for the structural evolution of Zanskar High

Himalaya. *In*: MACNIOCAILL, C. & RYAN, P. D. (eds) *Continental Tectonics*. Geological Society, London, Special Publications, **164**, 139–156.

SEARLE, M. P., SIMPSON, R. L., LAW, R. D., WATERS, D. J. & PARRISH, R. R. 2002. Quantifying displacement on the South Tibetan detachment normal fault, Everest massif, and the timing of crustal thickening and uplift in the Himalaya and South Tibet. *Journal of Nepal Geological Society*, **26**, 1–6.

SEARLE, M. P., SIMPSON, R. L., LAW, R. D., PARRISH, R. R. & WATERS, D. J. 2003. The structural geometry, metamorphic and magmatic evolution of the Everest massif, High Himalaya of Nepal-south Tibet. *Journal of the Geological Society, London*, **160**, 345–366.

SEEBER, L. & GORNITZ, V. 1983. River profiles along the Himalayan arc as indicators of active tectonics. *Tectonophysics*, **92**, 335–367.

SIMPSON, R. L. 2002. *Metamorphism, melting and extension at the top of the High Himalayan slab, Mount Everest region, Nepal and Tibet*. DPhil. thesis, Oxford University.

SIMPSON, R. L., PARRISH, R. R., SEARLE, M. P. & WATERS, D. J. 2000. Two episodes of monazite crystallization during metamorphism and crustal melting in the Everest region of the Nepalese Himalaya. *Geology*, **28**, 403–406.

SMITH, H. A. & BARRIERO, B. 1990. Monazite U-Pb dating of staurolite grade metamorphism in pelitic schists. *Contributions to Mineralogy and Petrology*, **105**, 602–615.

STEPHENSON, B. J., WATERS, D. J. & SEARLE, M. P. 2000. Inverted metamorphism and the Main Central Thrust: field relations and thermobarometric constraints from the Kishtwar Window, NW Indian Himalaya. *Journal of Metamorphic Geology*, **18**, 571–590.

STEPHENSON, B. J., SEARLE, M. P. & WATERS, D. J. 2001. Structure of the Main Central Thrust zone and extrusion of the High Himalayan crustal wedge, Kishtwar–Zanskar Himalaya. *Journal of Geological Society, London*, **158**, 637–652.

VANCE, D. & HARRIS, N. 1999. Timing of prograde metamorphism in the Zanskar Himalaya. *Geology*, **27**, 395–398.

VANNAY, J.-C. & GRASEMANN, B. 2001. Himalayan inverted metamorphism and syn-convergence extension as a consequence of a general shear extrusion. *Geological Magazine*, **138**, 253–276.

VANNAY, J.-C. GRASEMANN, B., RAHN, M., FRANK, W., CARTER, A., BAUDRAZ, V. & COSCA, M. 2004. Miocene to Holocene exhumation of metamorphic crustal wedges in the NW Himalaya: Evidence for tectonic extrusion coupled to fluvial erosion. *Tectonics*, **23**, TC1014.

VISKUPIC, K. & HODGES, K. V. 2001. Monazite–xenotime thermochronometry: methodology and an example from the Nepalese Himalaya. *Contributions to Mineralogy and Petrology*, **141**, 233–247.

VISONA, D. & LOMBARDO, B. 2002. Two-mica and tourmaline leucogranites from the Everest–Makalu region (Nepal-Tibet); Himalayan leucogranite genesis by isobaric heating? *Lithos*, **62**, 125–150.

WALKER, C. B., SEARLE, M. P. & WATERS, D. J. 2001. An integrated tectonothermal model for the evolution of the High Himalaya in western Zanskar with constraints from thermobarometry and metamorphic modeling. *Tectonics*, **20**, 810–833.

WALKER, J. D., MARTIN, M. W., BOWRING, S. A., SEARLE, M. P., WATERS, D. J. & HODGES, K. V. 1999. Metamorphism, melting and extension: Age constraints from the High Himalayan slab of Southeastern Zanskar and Northwestern Lahoul. *Journal of Geology*, **107**, 473–495.

WANG, Q., ZHANG, P., FREYMUELLER, J. T. *ET AL.* 2001. Present-day crustal deformation in China constrained by Global Positioning System measurements. *Science*, **294**, 574–577.

WEI, W., UNSWORTH, M., JONES, A. *ET AL.* 2001. Detection of widespread fluids in the Tibetan crust by magnetotelluric studies. *Science*, **292**, 716–718.

WEINBERG, R. F. & SEARLE, M. P. 1999. Volatile-assisted intrusion and autometasomatism of leucogranites in the Khumbu Himalaya, Nepal. *Journal of Geology*, **107**, 27–48.

WU, C., NELSON, K. D., WORTMAN, G. *ET AL.* 1998. Yadong cross-structure and South Tibetan Detachment in the east central Himalaya (89°–90°E). *Tectonics*, **17**, 28–45.

ZHAO, W., NELSON, K. D. and Team Project INDEPTH. 1993. Deep seismic reflection evidence for continental underthrusting beneath southern Tibet. *Nature*, **366**, 557–559.